Human Dicer helicase domain recruits PKR and dsRNA binding proteins during viral infection

Thomas C. Montavon[1,*], Morgane Baldaccini[1,*], Mathieu Lefèvre[1,*], Erika Girardi[1], Béatrice Chane-Woon-Ming[1], Mélanie Messmer[1], Philippe Hammann[2], Johana Chicher[2], Sébastien Pfeffer[1,‡]

[1] Université de Strasbourg, Architecture et Réactivité de l'ARN, Institut de Biologie Moléculaire et Cellulaire du CNRS, 2 allée Konrad Roentgen, 67084 Strasbourg France

[2] Université de Strasbourg, Institut de Biologie Moléculaire et Cellulaire du CNRS, Plateforme Protéomique Strasbourg – Esplanade, 2 allée Konrad Roentgen, 67084 Strasbourg France

*These authors contributed equally

‡ To whom correspondence should be addressed: spfeffer@unistra.fr

Abstract

The antiviral innate immune response mainly involves type I interferon (IFN) in mammalian cells. The contribution of the RNA silencing machinery remains to be established, but several recent studies indicate that the ribonuclease DICER can generate viral siRNAs in specific conditions. It has also been proposed that type I IFN and RNA silencing could be mutually exclusive antiviral responses. In order to decipher the implication of DICER during infection of human cells with the Sindbis virus, we determined its interactome by proteomics analysis. We show that DICER specifically interacts with several double-stranded RNA binding proteins and RNA helicases during viral infection. In particular, proteins such as DHX9, ADAR-1 and the protein kinase RNA-activated (PKR) are enriched with DICER in virus-infected cells. We demonstrate the importance of DICER helicase domain in its interaction with PKR and showed that it has functional consequences for the cellular response to viral infection.

33 ## Introduction

34 In mammalian cells, the main antiviral defense system involves the activation of a signaling
35 cascade relying on production of type I interferon (IFN I). This pathway depends on the
36 recognition of extrinsic signals or pathogen associated molecular patterns (PAMPs) by
37 dedicated host receptors. Double-stranded (ds) RNA, which can originate from viral replication
38 or convergent transcription, is a very potent PAMP and can be sensed in the cell by various
39 proteins among which a specific class of DExD/H-box helicases called RIG-I-like receptors
40 (RLRs) (Ivashkiv and Donlin, 2014). RLRs comprise RIG-I, MDA5 and LGP2 and transduce
41 viral infection signals to induce expression of IFN I cytokines that act in autocrine and paracrine
42 fashion. These cytokines then trigger the expression of hundreds of interferon stimulated genes
43 (ISGs) to stop the virus in its tracks (Borden et al, 2007). Among those ISGs, dsRNA-activated
44 protein kinase R (PKR) plays an important role in antiviral defense by blocking cellular and
45 viral translation upon direct binding to long dsRNA (Williams, 1999). PKR is a serine-threonine
46 kinase that dimerizes and auto-phosphorylates upon activation. It then phosphorylates
47 numerous cellular targets among which the translation initiation factor eIF2α, which results in
48 the inhibition of cap-dependent translation (Lemaire et al., 2008). Accordingly, translation of
49 many RNA viruses, including alphaviruses, is inhibited by PKR (Fros and Pijlman, 2016;
50 Pfaller et al., 2011; Ryman et al., 2002). PKR is also involved in other cellular pathways
51 including apoptosis, autophagy and cell cycle (Kim et al., 2014; Williams, 1999).

52 RNAi is another evolutionary conserved pathway triggered by long dsRNA sensing
53 (Meister and Tuschl, 2004). One key component in this pathway is the type III ribonuclease
54 DICER, which is also essential for micro (mi)RNA biogenesis (Hutvágner et al., 2001;
55 Wienholds et al., 2003). These small regulatory RNAs are sequentially produced by the two
56 ribonucleases DROSHA and DICER, before being loaded into an Argonaute (AGO) effector
57 protein in order to regulate their target mRNAs (Bartel, 2018). Whatever its substrate, be it long

58 dsRNA or miRNA precursor, DICER relies on interacting with co-factors to be fully functional.
59 In mammalian cells, the TAR-RNA binding protein (TRBP), a dsRNA binding protein
60 (dsRBP), was shown to play a role in the selection of DICER substrates, its stabilization, strand
61 selection and incorporation into AGO2 (Chendrimada et al., 2005). The interaction with TRBP
62 is well characterized and depends on the helicase domain of DICER and the third dsRNA
63 binding domain (dsRBD) of TRBP (Daniels et al., 2009). Another dsRBP, the protein activator
64 of interferon-induced protein kinase R (PACT), was also described as an important cofactor of
65 DICER. Although its function is not fully understood, PACT seems to also participate in
66 miRNA loading and strand selection (Heyam et al., 2015; Kok et al., 2007) *via* protein-protein
67 interaction between the DICER helicase domain and the third dsRBD of PACT (Lee et al.,
68 2006).

69 It is now common knowledge that RNAi is the main antiviral defense system in several
70 phyla such as plants, arthropods and nematodes (reviewed in (Guo et al., 2019)). However, its
71 exact contribution in the mammalian antiviral response remains unclear (Cullen, 2006; Maillard
72 et al., 2019; tenOever, 2016). Recent studies indicate that a functional antiviral RNAi does exist
73 in mammals in specific cases. A functional antiviral RNAi response was first detected in
74 undifferentiated mouse embryonic stem cells (Maillard et al., 2013) lacking the IFN response,
75 suggesting that these two pathways could be incompatible. Indeed, in mammalian somatic cells
76 deficient for MAVS or IFNAR, two components of the interferon response, an accumulation of
77 DICER-dependent siRNAs derived from exogenous long dsRNA was detected (Maillard et al.,
78 2016). In addition, the RLR LGP2 was found interacting with both DICER and TRBP, blocking
79 respectively siRNA production and miRNA maturation (Takahashi et al., 2018a, 2018b; van
80 der Veen et al., 2018). Moreover, AGO4 was recently shown to be involved in antiviral RNAi
81 against Influenza A virus (IAV), Vesicular stomatitis virus (VSV) and Encephalomyocarditis
82 virus (EMCV) (Adiliaghdam et al., 2020). Finally, viral suppressors of RNAi (VSRs) have been

83 shown to prevent DICER from playing an antiviral role in mammalian cells (Qiu et al., 2017,
84 2020). Nonetheless, several studies reported no detection of viral siRNAs in mammalian
85 somatic cells infected with several viruses (Girardi et al., 2013; Parameswaran et al., 2010;
86 Schuster et al., 2019). In somatic cells, only a helicase-truncated form of human DICER could
87 produce siRNAs from IAV genome (Kennedy et al., 2015), but it also turned out that these
88 siRNAs cannot confer an antiviral state (Tsai et al., 2018).

89 Based on these conflicting observations, we decided to study the involvement of DICER
90 during infection of human cells with the Sindbis virus (SINV). SINV is a member of the
91 *Togaviridae* family in the alphavirus genus, which is transmitted by mosquitoes to mammals
92 and can induce arthritogenic as well as encephalitic diseases (Griffin, 2007). It is widely used
93 as a laboratory alphaviruses model as it infects several cell types and replicates to high titers.
94 SINV has a positive stranded RNA genome of about 12 kb, which codes for two polyproteins
95 that give rise to non-structural and structural proteins, including the capsid. Moreover, upon
96 viral replication, a long dsRNA intermediate, which can be sensed by the host antiviral
97 machinery, accumulates. Of note, SINV dsRNA can be cleaved into siRNA in insects as well
98 as in human cells expressing the Drosophila DICER-2 protein (Girardi et al., 2015).
99 Nonetheless, although human DICER has the potential to interact with the viral RNA duplex,
100 we did not find evidence that SINV dsRNA could be processed into siRNAs in somatic
101 mammalian cells (Girardi et al., 2013, 2015). We thus hypothesized that specific proteins could
102 interfere with DICER during SINV infection by direct interaction and limit its accessibility
103 and/or activity. To address this hypothesis, we generated HEK293T cells expressing a tagged
104 version of human DICER that could be immunoprecipitated in mock or SINV-infected cells in
105 order to perform a proteomic analysis of its interactome. Among the proteins co-
106 immunoprecipitated with DICER and that were specifically enriched upon infection, we
107 identified dsRBPs such as ADAR1, DHX9, PACT and PKR. We further validated the direct

108 interaction between DICER and PKR upon SINV infection. We also demonstrated that the
109 interactions of the endogenous DICER with PKR, PACT and DHX9 could also be detected in
110 SINV-infected, but not mock-infected, HCT116 cells. We dissected the protein domains
111 necessary for this interaction and we found that DICER helicase domain plays a fundamental
112 role as a recruitment platform for PKR but also for other co-factors. Finally, we also show that
113 expression of a helicase-truncated version of DICER has a negative effect on SINV infection.
114 Our results indicate that DICER interactome is highly dynamic and directly link components
115 of RNAi and IFN pathways in modulating the cellular response to viral infection.
116

117 ## Results

118 **Establishment of a HEK293T cell line expressing FLAG-HA tagged DICER**

119 In order to be able to study the interactome of the human DICER protein during viral infection,
120 we transduced *Dicer* knock-out HEK293T cells (NoDice 2.20) (Bogerd et al., 2014a) with
121 either a lentiviral construct expressing a FLAG-HA-tagged wild type DICER protein
122 (FHA:DICER WT #4) or a construct without insert as a negative control (FHA:ctrl #1). After
123 monoclonal selection of stably transduced cells, we first characterized one clone of both
124 FHA:DICER WT and of the FHA:ctrl cell lines. We first confirmed that the expression of the
125 tagged version of DICER restored the miRNA biogenesis defect observed in the NoDice cells
126 (Fig. S1A). We then monitored the phenotype of these cells during SINV infection by using as
127 a readout of viral infection the modified version of SINV able to express GFP from a duplicated
128 sub-genomic promoter (SINV-GFP) (López et al, 2020). At 24 hours post-infection (hpi) and a
129 multiplicity of infection (MOI) of 0.02, the GFP fluorescence observed in FHA:DICER WT #4
130 cells and HEK293T cells was similar. However, the NoDice FHA:ctrl #1 cells displayed a
131 decrease in GFP signal (Fig. 1A). Western blot analysis of GFP expression confirmed the
132 observations by epifluorescence microscopy, *i.e.* a significantly lower accumulation of GFP in

133 the absence of the DICER protein (Fig. 1B). We therefore wished to confirm the effect of
134 DICER loss on SINV-GFP infection in another NoDice cell line, *i.e*. the NoDice clone 4.25
135 (Bogerd et al., 2014b), and in another clone of the NoDice 2.20 FHA:ctrl cells (NoDice
136 FHA:ctrl #2). We observed a similar decrease of SINV-GFP infection in NoDice 2.20 cells and
137 two independent NoDice FHA:ctrl clones compared to HEK293T cells as shown by GFP
138 microscopy (Fig. S1B), by titration of the virus (Fig. S1C) and by western blot analysis (Fig.
139 S1D). However, the independent NoDice 4.25 *Dicer* knock-out clone appeared mostly
140 unaffected compared to HEK293T cells in term of GFP accumulation and viral titer (Fig. S1B-
141 D). This suggests that, despite the observed slight effect on SINV-GFP in NoDice 2.20 cells
142 (Fig. 1), DICER antiviral effect is not reproductible in an independent clone and therefore could
143 not be generalized.

144 In order to evaluate whether different expression levels of DICER in a NoDice
145 background could rescue the SINV infection phenotype observed in HEK293T cells, we also
146 infected both the FHA:DICER WT polyclonal and an independent FHA:DICER WT clone
147 (FHA:DICER WT #17) with SINV-GFP (Fig. 1A and Fig. 1C-D). We confirmed that the GFP
148 fluorescence observed by microscopy (Fig. 1A), as well as the viral titers and the GFP protein
149 accumulation (Fig. 1C-D) in all tested FHA:DICER lines were comparable to the ones observed
150 in HEK293T cells. Moreover, there was no striking differences in AGO2 expression between
151 the FHA:DICER lines (Fig. 1D).

152 Altogether, these results indicate that the FHA-tagged DICER protein can functionally
153 complement the lack of DICER in terms of miRNA biogenesis (Fig. S1A) and can therefore be
154 used for proteomics studies. Moreover, because we could not observe significant differences in
155 terms of SINV infection (Fig. 1) between the different FHA:DICER clones tested, we decided
156 to select one line, namely FHA:DICER WT#4, for further analysis.

157

158 **Analysis of DICER interactome during SINV infection by mass spectrometry**

159 Our molecular tool being validated, we then focused on determining the interactome of
160 FHA:DICER during SINV infection. We wanted to look at DICER interactome at an early
161 infection time point to isolate cellular factors that could potentially modulate either DICER
162 accessibility or its effect on viral dsRNA. As SINV replicates quickly upon cellular entry, we
163 chose to set up the infection conditions to a duration of 6 hours at an MOI of 2.

164 We performed an anti-HA immunoprecipitation experiment (HA IP) coupled to label-
165 free LC-MS/MS analysis in FHA:DICER WT #4 cells either mock-infected or infected for 6 h
166 at an MOI of 2 with SINV-GFP. In parallel, we performed an anti-MYC immunoprecipitation
167 as a negative control (CTL IP). The experiments were performed in technical triplicate in order
168 to have statistically reproducible data for the differential analysis, which was performed using
169 spectral counts. Prior to the detailed analysis of the results, we verified that there was no
170 confounding factor in the experimentation by performing a Principal Component Analysis
171 (PCA). This allowed us to see that the replicates were very homogenous and that the different
172 samples were well separated based on the conditions.

173 To check the specificity of the HA immunoprecipitation, we first compared the proteins
174 identified in the HA IP with the ones identified in the CTL IP in mock-infected cells.
175 Differential expression analysis allowed us to calculate a fold change and an adjusted p-value
176 for each protein identified and to generate a volcano plot representing the differences between
177 HA and CTL IP samples. Applying a fold change threshold of 2 ((LogFC) > 1), an adjusted p-
178 value threshold of 0.05 and a cutoff of at least 5 spectral counts in the most abundant condition,
179 we identified 258 proteins differentially immunoprecipitated between the two conditions out of
180 1318 proteins (Fig. 2A and Supp. Table 1). Among these, 123 proteins were specifically
181 enriched in the HA IP. The most enriched protein was DICER, followed by its known co-factors
182 TRBP and PACT (also known as PRKRA) (Chendrimada et al., 2005; Lee et al., 2006). We

183 were also able to retrieve AGO2, indicating that the RISC loading complex was
184 immunoprecipitated and that proteins retrieved in our HA IP are specific to DICER
185 immunoprecipitation.

186 We next performed the differential expression analysis of proteins retrieved in the HA
187 IP in SINV-GFP compared to mock-infected cells. Among 1342 proteins, 296 were
188 differentially retrieved between conditions (Fig. 2B and Supp. Table 2). Of these, 184 proteins,
189 including viral ones, were at least 2-fold enriched in SINV-GFP-infected cells. GO-term
190 analysis showed a significant enrichment in RNA binding proteins including double-stranded
191 RNA binding proteins and RNA helicases (Fig. 2C). Among the RNA binding proteins
192 retrieved, the top and most specific DICER interactor is the interferon-induced, double-stranded
193 (ds) RNA-activated protein kinase PKR (also known as E2AK2), which is enriched more than
194 250 times in virus-infected cells (Fig. 2B and D). We were also able to identify the dsRNA-
195 specific adenosine deaminase protein ADAR-1 (also known as DSRAD), as well as PACT,
196 which were enriched 5.9 and 4.2 times respectively in SINV-GFP-infected cells compared to
197 mock-infected cells (Fig. 2B and D). Among the isolated RNA helicases, we identified the
198 ATP-dependent RNA helicase A protein DHX9, which is implicated in *Alu* element-derived
199 dsRNA regulation and in RISC loading (Aktaş et al., 2017; Robb and Rana, 2007). In order to
200 verify if the observed interactions were specific to SINV we performed the same experiments
201 with another virus of the *Togaviridae* family, the Semliki forest virus (SFV). In this analysis,
202 we were able to retrieve ADAR-1, DHX9, PACT and PKR, specifically enriched in SFV-
203 infected samples (Fig. S2 and Supp. Tables 3 and 4). These results show that these interactions
204 can be retrieved in *Togaviridae*-infected cells.

205 Taken together, our data indicate that several proteins interacting with DICER in virus-
206 infected cells are involved in dsRNA sensing and/or interferon-induced antiviral response.
207

208 **DICER and PKR interact *in vivo* in the cytoplasm during SINV infection**

209 To validate the LC-MS/MS analysis, we performed a co-immunoprecipitation (co-IP) followed
210 by western blot analysis in FHA:DICER WT #4 cells infected with SINV-GFP at an MOI of 2
211 for 6 h. Whereas TRBP interacted equally well with FHA:DICER in mock and SINV-GFP-
212 infected cells, ADAR-1, PKR, DHX9 and PACT were only retrieved in the HA IP in SINV-
213 infected cells (Fig. 3A). We verified that these interactions could also be observed at a later
214 time post-infection by performing the HA IP in FHA:DICER WT #4 cells infected with SINV-
215 GFP for 24 h at an MOI of 0.02. This indicates that the specific interactions between DICER
216 and ADAR-1, DHX9, PACT or PKR occur at an early stage of the SINV infection and remain
217 stable in time in virus-infected cells (Fig. S3A).

218 In order to verify whether these interactions were mediated by RNA, we performed an
219 anti-HA co-IP experiment on an RNase A/T1 treated total extract from FHA:DICER WT #4
220 cells infected with SINV-GFP at an MOI of 2 for 6h. We confirmed the efficiency of the RNase
221 treatment by ethidium bromide staining visualisation of total RNA on an agarose gel (Fig. S3B).
222 TRBP equally interacted with FHA:DICER, with or without RNase treatment, in mock and
223 SINV-GFP-infected cells (Fig. 3B). Instead, the virus-induced interactions between DICER and
224 PKR or PACT upon SINV-GFP infection were almost totally lost in the RNase-treated samples.
225 Upon virus infection, PKR is phosphorylated to be activated and exert its antiviral function
226 (Lemaire et al., 2008). Using an antibody targeting the phosphorylated form of PKR (p-PKR),
227 we looked for p-PKR before and after RNase treatment. The virus-enriched interactions
228 between DICER and p-PKR or DHX9 were completely lost upon RNase treatment. These
229 results therefore indicate that RNA molecules (either single- or double-stranded) facilitate
230 DICER interaction with DHX9, PACT and PKR and its active form, although the complex may
231 also partially interact in an RNA-independent manner.

232 Because of the involvement of PKR in antiviral response (García et al., 2007) and the
233 fact that it shares common co-factors with DICER, namely TRBP and PACT (Haase et al.,
234 2005; Patel et al., 2000), we decided to focus our analysis on the DICER-PKR interaction. To
235 confirm the biological relevance of this interaction, we first performed a reverse co-IP to
236 immunoprecipitate the endogenous PKR protein in HEK293T cells infected or not with SINV-
237 GFP. While PACT interacted with PKR both in mock and in SINV-GFP-infected cells as
238 expected (Fig. 3C lower panel), DICER co-immunoprecipitated with the endogenous PKR only
239 in virus-infected cells as previously observed (Fig. 3C upper panel).
240 To further determine whether DICER and PKR could directly interact *in vivo*, we set up
241 a bi-molecular fluorescent complementation assay (BiFC) experiment (Lepur et al., 2016). To
242 this end, we fused the N- or C-terminal halves of the Venus protein ($^{N\text{-}ter}$Venus or $^{C\text{-}ter}$Venus) to
243 DICER and to PKR but also to TRBP and PACT. Since we showed above that an N-terminally
244 tagged DICER was functional, we fused the Venus fragments at the N-terminal end of DICER.
245 For the other three proteins, we fused the Venus fragments at the N- or C-terminus and selected
246 the best combination. To avoid interaction with the endogenous DICER and PKR proteins, we
247 conducted all BiFC experiments in NoDice/ΔPKR HEK293T cells (Kennedy et al., 2015). In
248 order to control the BiFC experiments, we chose to exploit the well characterized DICER-
249 TRBP interaction, which is known to occur via the DICER DEAD-box helicase domain
250 (Daniels et al., 2009). We therefore used the wild-type DICER protein as a positive control and
251 a truncated version of DICER protein lacking part of this helicase domain and called DICER
252 N1 (Kennedy et al., 2015) as a negative control (Fig. S3C). We first confirmed the expression
253 of the tagged proteins by western blot analysis (Fig. S3D) and then, we tested the interactions
254 between DICER and TRBP or PACT or PKR. We co-transfected the Venus constructs for 24 h
255 and then infected cells with SINV or not for 6 h at a MOI of 2. A comparable fluorescent signal
256 was observed both in mock- and SINV-infected cells when $^{N\text{-}ter}$Venus:DICER was co-

257 transfected with either PACT or TRBP fusion construct (Fig. 3D). Although we initially
258 expected an increase of the Venus fluorescence in SINV-infected cells, overall we observed a
259 similar signal for the DICER-PKR interaction both in mock- and SINV-infected cells, probably
260 due to the fact that both proteins are transiently overexpressed in this experiment.

261 As a control and to rule out any aspecific interactions between the different proteins
262 tested, we also monitored the DICER-N1-TRBP interaction by BiFC. As expected, no
263 fluorescent signal was observed in cells co-transfected with $^{N\text{-}ter}$Venus:DICER N1 and
264 TRBP:Venus$^{C\text{-}ter}$ (Fig. S3E), confirming that DICER helicase domain is required for its
265 interaction with TRBP (Daniels et al., 2009) and validating the specificity of the BiFC
266 approach.

267 To further confirm that the absence of PKR did not influence the interactions of TRBP
268 or PACT with DICER, we also performed a BiFC analysis in HEK293T cells. After verifying
269 that in this context as well, fusion proteins were expressed as expected (Fig. S3F), we observed
270 that the results were similar as in NoDiceΔPKR cells (Fig. S3G).

271 To gain more insight into the subcellular localization of these interactions during SINV
272 infection, we performed the BiFC experiments, fixed the cells and observed them under a
273 confocal microscope. We observed a cytoplasmic fluorescent signal for DICER-TRBP and
274 DICER-PACT interactions (Fig. 3E upper and middle panels), which is in agreement with their
275 canonical localization for the maturation of most miRNAs (Bernstein et al., 2001; Hutvágner
276 et al., 2001). Similarly, co-transfection of DICER and PKR led to a strong Venus signal
277 homogeneously distributed in the cytoplasm (Fig. 3E lower panel).

278 Collectively, these results formally confirm that DICER interacts with several RNA
279 helicases and dsRNA-binding proteins in virus-infected cells, among which PKR, and that for
280 the latter this interaction occurs in the cytoplasm.

281

282 **DICER interactome changes upon SINV infection are not cell-type specific**

283 To further validate our previous DICER interactome results and generalize them to another
284 biological system, we performed co-IP experiments on the endogenous DICER in a different
285 cell type. To this end, the FLAG-HA-GFP tag was knocked into (KI) the *Dicer* locus in human
286 colon carcinoma cells (HCT116) by CRISPR-Cas9-mediated homologous recombination (Fig.
287 S4A-C). A guide RNA (gRNA) targeting the region corresponding to Dicer ATG and a DNA
288 template for homologous recombination bearing the FLAG-HA-GFP sequence surrounded by
289 the upstream and downstream arms of Dicer were used to generate the resulting cell line
290 referred to as HCT116 KI-DICER cells. The expected insertion of the tag in one of the two
291 Dicer allele was assessed by PCR amplification and Sanger sequencing (Fig. S4A-C). In
292 agreement, we could detect two bands for DICER protein by western blot in the HCT116 KI-
293 DICER cells, which confirmed that this cell line is heterozygous (Fig. 4A).

294 We additionally verified the expression of specific DICER-interacting proteins, such as
295 AGO2, PKR or TRBP, in HCT116 KI-DICER cells compared to the parental HCT116 cells
296 and to HEK293T cells (Fig. 4A). We also measured the production of mature miRNAs, such
297 as miR-16, by northern blot analysis and confirmed that miRNA expression is maintained in
298 HCT116 KI-DICER cells (Fig. 4B). Of note, the GFP inserted at the *Dicer* locus could not be
299 detected by epifluorescence microscopy in the HCT116 KI-DICER cells, which probably
300 reflects the low abundance of the DICER protein.

301 We then determined whether SINV-GFP infection was comparable in HCT116 cells and
302 HEK293T cells. We infected HCT116, HCT116 KI-DICER and HEK293T cells with SINV-
303 GFP at three different MOI (0.02, 0.1 and 1) and measured GFP fluorescence by microscopy at
304 24 hpi (Fig. 4C). Both HCT116 and HCT116 KI-DICER cells expressed GFP upon infection
305 with SINV-GFP, although with a lower intensity than HEK293T cells. We also verified by
306 western blot analysis the accumulation of GFP and the phosphorylation of both PKR and eIF2α

307 upon SINV-GFP infection of HCT116 KI-DICER and HEK293T cells (Fig. S4D) and chose as
308 optimal SINV-GFP condition of infection in HCT116 KI-DICER cells the MOI of 0.1 for 24h.
309 To validate the DICER interactions observed in HEK293T FHA:DICER cells, we then
310 performed anti-HA co-IP experiments followed by western blot analysis in HCT116 KI-DICER
311 cells infected or not with SINV-GFP. We successfully retrieved TRBP interacting with DICER
312 in both mock and infected cells, whereas DHX9, PKR (phosphorylated or not) and PACT were
313 only retrieved in the HA IP in infected cells (Fig. 4D). These results not only confirm that the
314 endogenous DICER specifically interacts with DHX9, PACT and PKR upon SINV infection,
315 but also that these interactions are not restricted to one specific cell type.
316
317 **The helicase domain of DICER is required for its interaction with PKR**
318 Even though DICER and PKR are likely brought together by RNA, specific protein domains
319 might be involved in stabilizing the complex. We therefore next determined the domain of
320 DICER required for its interaction with PKR. Since its helicase domain was previously shown
321 to be involved in the interaction with TRBP and PACT (Daniels et al., 2009; Lee et al., 2006),
322 we speculated that it could also be implicated in binding PKR. To test this hypothesis, we cloned
323 several versions of DICER proteins wholly or partly deleted of the helicase domain (Fig. 5A
324 DICER N1 and N3). In addition, we also cloned the helicase domain alone (Fig. 5A DICER
325 Hel.) and a DICER variant deleted of its C-terminal dsRNA binding domain (Fig. 5A DICER
326 ΔdsRBD) since this domain could also be involved in protein-protein interaction (Doyle et al.,
327 2013; Lambert et al., 2016). We then transfected the different versions of DICER WT and the
328 deletion mutant constructs in NoDice cells. In mock and SINV-GFP infected cells, whole cell
329 extracts were subjected to anti-HA and anti-MYC (CTL) IP. TRBP was retrieved in both
330 conditions with DICER WT, Hel. and ΔdsRBD (Fig. 5B and 5C). In mock cells, PACT and
331 PKR were only found weakly interacting with DICER WT (Fig. 5B). In SINV-infected cells,

332 we observed that similar to TRBP and to a lesser extent PACT, N1 and N3 mutations strongly
333 reduced the binding of DICER with PKR (Fig. 5C lanes 2-3 and 7-8). Importantly, we also
334 noted that the helicase domain alone could bind PKR, TRBP and PACT (Fig. 5C lanes 4 and
335 9). Moreover, the deletion of the dsRNA binding domain of DICER did not affect its interaction
336 with TRBP, PACT and PKR (Fig. 5C lanes 5 and 10). We also looked for p-PKR in our co-IP
337 (Fig. 5C panel p-PKR). We noticed that only WT DICER and its helicase domain were able to
338 interact with p-PKR (Fig. 5C lanes 1&6 and 4&9). The fact that DICER ΔdsRBD did not
339 interact with p-PKR (Fig. 5C lanes 5&10) is striking but could indicate that the phosphorylation
340 of PKR may induce conformation changes preventing its interaction with some domains of
341 DICER. These results reveal that, like for TRBP and PACT, the helicase domain of DICER is
342 required for DICER-PKR/p-PKR interaction during SINV infection.

343 In order to confirm these co-IP experiments, we next decided to perform BiFC
344 experiments using the same conditions as previously. In both mock and SINV-infected cells,
345 only the combinations of DICER WT-PKR and DICER ΔdsRBD-PKR showed a strong Venus
346 signal, while neither DICER N1 nor N3 constructs revealed an interaction with PKR (Fig. 5D).
347 In contrast, the DICER Hel. construct did not seem to interact with PKR in mock-infected cells
348 but appeared to do so in SINV-infected cells as a faint Venus signal could be observed. These
349 results therefore confirmed the co-IP observations for the DICER-PKR interaction. In addition,
350 we also performed a BiFC experiment using the different DICER constructs with TRBP or
351 PACT. Altogether, the BiFC results mostly fitted with the co-IP experiment for the DICER-
352 TRBP (Fig. S5A) and DICER-PACT (Fig. S5B) interactions. TRBP indeed did not seem to
353 interact with the DICER N1 and only slightly with the DICER N3. However, PACT interaction
354 was lost with DICER N1, but not with DICER N3 in mock- and SINV-infected cells (Fig. S5B
355 third panel). This result may be explained by the fact that DICER interacts with PACT *via* the
356 helicase and DUF domains, whereas only the DICER helicase domain is required for its

357 interaction with TRBP (Daniels et al., 2009; Lee et al., 2006). In agreement, the Venus signal
358 observed between the DICER Hel. and PACT seemed weaker than the one we observed with
359 TRBP (Fig. S5A and B fourth panels).

360 Taken together these results indicate that DICER interacts with both PKR and its
361 phosphorylated form during SINV infection and that this interaction requires the helicase
362 domain of DICER.

363

364 **Functional importance of DICER helicase domain during SINV infection**

365 We finally sought to study the functional role of DICER-PKR interaction during viral infection.
366 For this purpose, we decided to use DICER helicase deletion mutants to study SINV infection.
367 To do so, we first generated NoDice HEK293T cells stably expressing FHA-tagged DICER N1
368 (FHA:DICER N1) by lentiviral transduction. As for the FHA:DICER WT cell line, we first
369 selected a clone expressing the tagged DICER N1 at a level similar level to the endogenous
370 DICER protein in HEK293T cells (Fig. 6A). DICER N1 protein has been shown to still be able
371 to produce miRNAs (Kennedy et al., 2015). We thus verified by northern blot analysis that
372 DICER N1 is indeed able to process miRNAs similarly to WT DICER in HEK 293T and
373 FHA:DICER cells, thereby validating the functionality of the tagged protein (Fig. 6B). We next
374 infected HEK293T, FHA:DICER WT #4 and FHA:DICER N1 #6 cells with SINV-GFP and
375 measured virus accumulation by assessing GFP expression by microscopy analysis.
376 Interestingly, the GFP protein level was drastically reduced in FHA:DICER N1 #6 cells
377 compared to FHA:DICER WT #4 and HEK293T cells (Fig. 6C). Encouraged by this
378 observation, we decided to infect with SINV-GFP additional DICER deletion mutants, namely
379 N3 and Hel. We generated stable cell lines for these various mutants by lentiviral transduction
380 in the NoDice 2.20 background and infected those cells with SINV-GFP at an MOI of 0.02 for
381 24h. We verified by western blot analysis that all selected DICER mutant clones, namely N1

382 #6, N3 #2.13 and Hel. #2.6, expressed the tagged protein at the expected size and at levels
383 mostly similar to the FHA:DICER WT #4 line (Fig. 6D, first two panels). We also verified the
384 DICER mutants contribution to the endogenous miRNA biogenesis by performing a northern
385 blot analysis on miR-16 accumulation (Fig. S6A).

386 We additionally verified the impact of these DICER mutants on SINV-GFP infection
387 by measuring the GFP intensity of fluorescence by microscopy (Fig. S6B). Our results indicated
388 that GFP accumulation is similar in HEK293T, NoDice 2.20, FHA:DICER WT, Hel. and ctrl
389 cells. However, almost no fluorescence was detected in FHA:DICER N1 #6 and N3 #2.13 cells
390 compared to HEK293T cells (Fig. S6B). The reduction of virus-encoded GFP accumulation
391 and viral production were confirmed by western blot (Fig. 6D) and by plaque assay,
392 respectively (Fig. 6E).

393 Altogether, these results therefore indicate that expressing a helicase truncated
394 version of DICER, which is unable to interact with PKR, appears to confer an antiviral
395 phenotype to SINV infection.

396

397 **Discussion**

398 The role of DICER in antiviral defense in human cells remains a topic of intense discussion
399 (Cullen et al., 2013; Maillard et al., 2013, 2019; Cullen, 2017). In particular there have been
400 contradictory reports regarding its capacity to produce siRNAs from viral RNAs (Bogerd et al.,
401 2014a; Parameswaran et al., 2010; Donaszi-Ivanov et al., 2013; Backes et al., 2014). These
402 observations could be due to the fact that several mammalian viruses potentially encode VSR
403 proteins, thereby masking the effect of RNAi (Li et al., 2013, 2016; Maillard et al., 2013; Qiu
404 et al., 2017, 2020). Another putative but non-exclusive explanation could be that there is a
405 mutual regulation of type I IFN and RNAi pathways (Berkhout, 2018; Takahashi and Ui-Tei,
406 2020). Thus, it has already been shown that PACT can regulate MDA5 and RIG-I during virus

407 infection and therefore the induction of type I IFN response (Kok et al., 2011; Lui et al., 2017).
408 To date, it is not clear whether the activity of the DICER protein as well could be regulated by
409 potential interactors, or inversely whether it could itself modulate the activity of proteins
410 involved in the IFN pathway. To answer this question, we determined the changes in the
411 interactome of human DICER upon SINV and SFV infection. This analysis allowed us to reveal
412 that a lot of proteins associating with DICER during viral infection are dsRNA-binding proteins
413 and RNA helicases. A number of these proteins are known to be involved in antiviral defense
414 pathways, thereby indicating the possible formation of one or several complexes between
415 DICER and these proteins, which are very likely brought together by the accumulation of
416 dsRNA during virus infection.

417 Among these proteins, we chose to focus on the well-known ISG PKR, which is
418 involved in many cellular pathways such as apoptosis, cellular differentiation, development and
419 antiviral defense (Clemens, 1997; Gal-Ben-Ari et al., 2018; Kim et al., 2014; Lemaire et al.,
420 2008). PKR is one of the main actors of the Integrative Stress Response (ISR) in human cells,
421 and its activation or inhibition needs to be tightly regulated in order to have a properly balanced
422 response to stress. Our results indicate that DICER interacts via its helicase domain with PKR
423 in the cytoplasm during SINV infection. The helicase domain of DICER, which is also required
424 for its interaction with TRBP and PACT, belongs to the helicase superfamily 2, which is also
425 found in RLRs such as RIG-I, MDA5 or LGP2 (Ahmad and Hur, 2015; Fairman-Williams et
426 al., 2010). These proteins act as sensors of viral infection and through the activation of proteins
427 such as MAVS, mediate the induction of type I IFN pathway (Ahmad and Hur, 2015). We
428 hypothesize that even though the human DICER helicase has evolved mainly to act in
429 miRNA/siRNA pathway, it still retained the capacity to act as an RLR. However, as opposed
430 to RIG-I and MDA5, our data suggest that DICER would act more as an inhibitor rather than

431 inducer of the immune response. Therefore, we propose that this domain serves as a platform
432 for the recruitment of different proteins to diversify the function of DICER.

433 One such regulatory effect appears to be on the antiviral activity of PKR, as cells
434 expressing a truncated form of DICER unable to interact with PKR become resistant to SINV
435 infection. This is in agreement with previous observations that ectopic expression of the
436 *Drosophila* DICER2 protein in human cells perturbs IFN signaling pathways and antagonizes
437 PKR-mediated antiviral immunity (Girardi et al., 2015). The exact mechanism involved is still
438 unclear and will require further work, but it seems that the two proteins are likely brought
439 together *via* their interaction with RNA, most probably of viral origin. Indeed, we showed that
440 the co-IP interaction was partially RNase sensitive. However, we confirmed that the interaction
441 is not artificially created during the co-immunoprecipitation procedure, since we could show
442 that DICER and PKR interact in BiFC assay, a technique that favors the detection of direct
443 interactions (Lepur et al., 2016). Most of the time, the inhibition of PKR activity relies on its
444 inhibition to bind to dsRNA or to auto-phosphorylate. For example, the human tRNA-
445 dihydrouridine synthase 2 (hDus2) binds the first dsRBD of PKR and prevents its activation
446 (Mittelstadt et al., 2008). TRBP binds dsRNAs but also PKR directly hindering its dimerization.
447 In normal condition, TRBP is also associated with PACT thus preventing PKR activation by
448 PACT (Park et al., 1994; Nakamura et al., 2015; Daher et al., 2009; Singh et al., 2011). Since
449 we showed that DICER can bind the activated phospho-PKR, we hypothesize that this
450 interaction does not result in the inhibition of PKR autophosphorylation. In fact, in condition
451 of infection with a high virus dose, we showed that phospho-PKR levels are similar in cells
452 expressing DICER WT or helicase deletion mutants N1 and N3, but the activated PKR does
453 not associate with these truncated versions of DICER. Therefore, one possibility could be that
454 DICER interaction with PKR prevents the latter from acting upon some of its targets, which
455 remain to be identified, to fine-tune the antiviral response.

456 As of now, we cannot formally rule out that the effect of DICER on PKR is mediated
457 by other proteins. TRBP and PACT have been shown to regulate PKR activity, the former
458 normally acting as a repressor and the latter as an activator (Nakamura et al., 2015; Patel et al.,
459 2000; Singh et al., 2011). Interestingly, in lymphocytic Jurkat cells infected by HIV-1, PACT
460 can also act as a repressor of PKR (Clerzius et al., 2013). It is thus tempting to speculate that
461 these two proteins participate in the formation of the DICER-PKR complex. However, our
462 results show that this may not necessarily be the case. Indeed, in the BiFC experiment, the
463 DICER N3 mutant still interacted with PACT but not with PKR indicating that PACT binding
464 is not sufficient to confer the association with PKR.

465 Besides PKR, other proteins were specifically enriched upon viral infection in the
466 DICER IP. These are also interesting candidates to explain the putative regulatory role of
467 DICER. Among these proteins, DHX9 and ADAR-1 are especially intriguing. DHX9, also
468 known as RNA helicase A (RHA), associates with RISC, helping the RISC loading (Robb and
469 Rana, 2007). Moreover, DHX9 is directly involved in removing toxic dsRNAs from the cell to
470 prevent their processing by DICER (Aktaş et al., 2017). It has also been implicated in HIV-1
471 replication and knockdown of DXH9 leads to the production of less infectious HIV-1 virions
472 (Li et al., 1999; Fujii et al., 2001; Roy et al., 2006). Finally, DXH9 interacts with and is
473 phosphorylated by PKR in mouse embryonic fibroblasts. This phosphorylation precludes the
474 association of DHX9 with RNA, thus inhibiting its proviral effect (Sadler et al., 2009). In light
475 of these observations and ours, we can speculate that the inhibitory effect of DICER on PKR
476 activity could also be linked to DHX9 phosphorylation. ADAR-1 is one of the well-known
477 RNA-editing factors (Herbert et al., 1997). ADAR-1 is linked to both miRNA biogenesis (Iizasa
478 et al., 2010; Ota et al., 2013; Yang et al., 2006) and virus infection. Indeed, ADAR-1 has an
479 antiviral effect against Influenza virus, but most of the time, its depletion leads to a decrease of
480 the viral titer, as was reported for VSV or HIV-1 (Li et al., 2010; Samuel, 2011). It has been

481 shown that ADAR-1 and PKR interact directly during HIV-1 infection. This interaction triggers
482 the inhibition of PKR activation, and thus a reduction of eIF2α phosphorylation leading to an
483 increase of virus replication (Pfaller et al., 2011; Clerzius et al., 2009). Interestingly, over-
484 expression of ADAR-1 enhances drastically the replication of the alphaviruses Chikungunya
485 virus (CHIKV), and Venezuelan equine encephalitis virus (VEEV) most likely by interfering
486 with the IFN induction (Schoggins et al., 2011).

487 Finally, we cannot formally rule out that the virus resistance phenotype of the DICER
488 N1 and N3 cell lines is due to an increased processivity of these truncated proteins on long
489 dsRNA substrates (Kennedy et al., 2015), which would render DICER RNAi proficient.
490 However, PKR is still expressed in these cells, and is therefore expected to be predominant over
491 DICER for viral dsRNA sensing. It is nonetheless possible that its interaction with several
492 dsRNA binding proteins could also participate in limiting the efficiency of the helicase domain
493 of DICER, on top of its intrinsic lack of processivity (Chakravarthy et al., 2010).

494 Deciphering the exact role of human DICER protein during virus infection is a
495 challenging task and additional studies will be required to get a global picture. Nevertheless, by
496 assessing the interactome of this protein during SINV infection, we have unveiled a new role
497 for the helicase domain of DICER in regulating the cellular response to viral infection.

498

499 ## Material and methods

500 **Plasmids, cloning and mutagenesis**

501 Plasmids used for BiFC experiments were a gift from Dr. Oliver Vugrek from the Ruđer
502 Bošković Institute and described in (Lepur et al., 2016). The cDNAs of TRBP, PACT and PKR
503 were respectively amplified from (pcDNA-TRBP Addgene #15666) (Kok et al., 2007),
504 (pcDNA-PACT Addgene #15667) (Kok et al., 2007), (pSB819-PKR-hum Addgene #20030)
505 (Elde et al., 2009), and cloned into the four pBiFC vectors by Gateway recombination. DICER

506 N1, N3 Hel. and ΔdsRBD were generated by PCR mutagenesis from pDONR-DICER described
507 in (Girardi et al., 2015) and cloned into the four pBiFC and pDEST-FHA vectors by Gateway
508 recombination. plenti6 FHA-V5 vector was modified from plenti6-V5 gateway vector (Thermo
509 Fisher scientific V49610) by Gibson cloning. DICER WT, N1 from pDONOR plasmids were
510 cloned into plenti6 FHA-V5 by Gateway recombination. All primers used are listed in Supp.
511 Table 5.
512
513 **Cell lines**
514 HEK293T, HEK293T/NoDice (2.20 and 4.25), and HEK293T/NoDiceΔPKR cell lines were a
515 gift from Pr. Bryan Cullen and described in (Bogerd et al., 2014b; Kennedy et al., 2015).
516 HCT116 cell line was a gift from Dr. Christian Gaiddon.
517

518 **Generation of Flag-HA-GFP-DICER knock-in cell line by CRISPR/Cas9**

519 To generate the knock-in cell line, the sequence of Flag-HA-GFP was amplified by PCR from
520 the Flag-HA-GFP plasmid (Meister et al., 2005). DNA sequences corresponding to 1 Kb
521 upstream (left homology arm) and downstream (right homology arm) the starting codon (ATG)
522 of DICER gene were amplified from HCT116 cell genomic DNA using primer pairs listed in
523 Supp. Table 5. The three PCR products were gel-purified and cloned into a linearized pUC19
524 by In-fusion cloning (Clontech) to obtain the template for homologous recombination
525 (LarmDICER-FlagHAGFP-RarmDICER).

526 Design of the guide RNA targeting the region between Dicer 5'-UTR and its first coding exon
527 for CRISPR/Cas9 mediated knock-in was carried out using the CRISPOR Design Tool
528 (Concordet and Haeussler, 2018). Annealed oligonucleotide corresponding to the gRNA (Supp.

529 Table 5) were cloned into the vector pX459 (Addgene #48139) which also encodes *S. pyogenes*
530 Cas9 with 2A-Puro.
531 The sequence of the donor plasmid was additionally mutagenized to disrupt the PAM sequence
532 of the right homology arm to avoid its cleavage by the gRNA.
533 To obtain the knock-in (KI) cell line, 5 x 10^5 HCT116 cells were seeded in a 6 well plate with
534 Dulbecco's modified Eagle medium (DMEM, Gibco®, Life Technologies) supplemented with
535 10% fetal bovine serum (FBS, Clontech) in a humidified atmosphere of 5% CO_2 at 37°C and
536 transfected after 24 hours with the pX459-gRNADicerNterm-Cas9-2A-Puro plasmid and the
537 Leftarm-FlagHAGFP-RightarmDICER donor plasmids at the ratio of 1 to 1 (6 micrograms
538 plasmids in total) using Lipofectamine 2000 according to the manufacturer instructions. 24
539 hours later, puromycin (1mg/mL) was added to the cells to increase the KI efficiency and
540 genomic DNA was isolated from individual colonies few days later.
541 The presence of the Flag-HA-GFP tag in frame with hDICER coding sequence was confirmed
542 by sequencing PCR amplicon from KI cell gDNA. Expression of Flag-HA-GFP N-terminal
543 tagged Dicer protein in the KI cells was confirmed by western blot.
544
545 **Cell culture and transfection**
546 Cells were maintained in Dulbecco's modified Eagle medium (DMEM, Gibco®, Life
547 Technologies) supplemented with 10% fetal bovine serum (FBS, Clontech) in a humidified
548 atmosphere of 5% CO_2 at 37°C. Transfection was performed using Lipofectamine 2000
549 (Invitrogen, ThermoFisher Scientific) according to the manufacturer's instructions.
550
551 **Lentivirus production and generation of stable cell lines**
552 The lentiviral supernatant from single transfer vector was produced by transfecting HEK293T
553 cells (ATCC® CRL-3216™) with 20 μg of the transfer vector, 15 μg of pMDLg/p RRE and 10

554 μg of pRSV-Rev packaging plasmids (Addgene #12251 and Addgene #12253) and the pVSV
555 envelope plasmid (Addgene #8454) using Lipofectamine 2000 (Invitrogen, ThermoFisher
556 Scientific) reagent according to the manufacturer's protocol. Standard DMEM (Gibco®, Life
557 Technologies) medium supplemented with 10% Fetal bovine serum (FBS, Gibco®, Life
558 Technologies) and 100 U/mL of penicillin-Streptomycin (Gibco®, Life Technologies) was
559 used for growing HEK293T cells and for lentivirus production. One 10 cm plate of HEK293T
560 cells at 70-80% confluency was used for the transfection. The medium was replaced 8 hours
561 post-transfection. After 48 hours the medium containing viral particles was collected and
562 filtered through a 0.45μm PES filter. The supernatant was directly used for transfection or
563 stored at -80°C. A 6 well plate of HEK293T/NoDice cells at 80% confluency was transduced
564 using 600 μL of lentiviral supernatant either expressing FHADICER, N1 or empty vector,
565 supplemented with 4 ug/mL polybrene (Sigma) for 6 hours. The transduction media was then
566 changed with fresh DMEM for 24 hours and the resistant cell clones were selected for about 6
567 weeks with blasticidin (15 μg/mL) and subsequently maintained under blasticidin selection.
568
569 **Viral stocks, virus infection**
570 Viral stocks of SINV or SINV-GFP were produced as described in (Girardi et al., 2015). Cells
571 were infected with SINV or SINV-GFP at an MOI of 0.02, 0.1, 1 or 2 and samples were
572 collected at different time points as indicated in the figure legends.
573
574 **Analysis of viral titer by plaque assay**
575 Vero R cells were seeded in 96-well plates format and were infected with 10-fold serial
576 dilutions infection supernatants for 1 hour. Afterwards, the inoculum was removed, and cells
577 were cultured in 2.5% carboxymethyl cellulose for 72 hours at 37°C in a humidified atmosphere

578 of 5% CO_2. Plaques were counted manually under the microscope and viral titer was calculated
579 according to the formula: *PFU/mL = #plaques/ (Dilution*Volume of inoculum)*
580
581 **Western blot analysis**
582 Proteins were extracted from cells and homogenized in 350 µL of lysis buffer (50 mM Tris-
583 HCl pH 7.5, 150 mM NaCl, 5 mM EDTA, 1% Triton X-100, 0.5% SDS and Protease Inhibitor
584 Cocktail (complete Mini; Sigma Aldrich)). Proteins were quantified by the Bradford method
585 and 20 to 30 µg of total protein extract were loaded on 4-20% Mini-PROTEAN® TGX™
586 Precast Gels (Bio-Rad). After transfer onto nitrocellulose membrane, equal loading was verified
587 by Ponceau staining. For PVDF membrane, equal loading was verified by Coomassie staining
588 after transfer and blotting. Membranes were blocked in 5% milk and probed with the following
589 antibodies: anti-hDicer (1:500, F10 Santa Cruz sc-136979) and anti-hDicer (1:1000, A301-
590 937A Bethyl), anti-TRBP (1:500, D-5 Santa Cruz sc-514124), anti-PKR (1:2500, Abcam
591 ab32506), anti-PACT (1:500, Abcam, ab75749), anti-HA (1:10000, Sigma, H9658), anti-
592 DHX9 (1:500, Abcam ab26271), anti-p-eIF2a (1:1000, Ser-52 Santa Cruz sc-601670), anti-
593 hADAR-1 (1:500 Santa Cruz sc-271854) anti-p-PKR (1:1000 Abcam ab81303) anti-GFP
594 (1:10000, Roche 11814460001) and anti-Tubulin (1:10000, Sigma T6557). Detection was
595 performed using Chemiluminescent Substrate (Pierce, ThermoFisher Scientific) and visualized
596 on a Fusion FX imaging system (Vilber).
597
598 **RNA extraction and northern blot analysis**
599 Total RNA was extracted using Tri-Reagent Solution (Fisher Scientific; MRC, Inc) according
600 to the manufacturer's instructions. Northern blotting was performed on 10 µg of total RNA.
601 RNA was resolved on a 12% urea-acrylamide gel, transferred onto Hybond-NX membrane (GE
602 Healthcare). RNAs were then chemically cross-linked to the membrane during 90 min at 65°C

603 using 1-ethyl-3-[3-dimethylaminopropyl]carbodiimide hydrochloride (EDC) (Sigma Aldrich).
604 Membranes were prehybridized for 30 min in PerfectHyb™ plus (Sigma Aldrich) at 50°C.
605 Probes consisting of oligodeoxyribonucleotides (see Supplementary Table 2) were 5′-end
606 labeled using T4 polynucleotide kinase (ThermoFisher Scientific) with 25 μCi of [γ-32P]dATP.
607 The labeled probe was hybridized to the blot overnight at 50°C. The blot was then washed twice
608 at 50°C for 20 min (5× SSC/0.1% SDS), followed by an additional wash (1× SSC/0.1% SDS)
609 for 5 min. Northern blots were exposed to phosphorimager plates and scanned using a
610 Bioimager FLA-7000 (Fuji).
611
612 **Immunoprecipitation**
613 Immunoprecipitation experiments were carried out either on tagged proteins or on endogenous
614 proteins.
615 *Tagged proteins*: Cells were harvested, washed twice with ice-cold 1× PBS (Gibco®, Life
616 Technologies), and resuspended in 550 μL of lysis buffer (50 mM Tris-HCl pH 7.5, 140 mM
617 NaCl, 1.5 mM $MgCl_2$, 0.1% NP-40), supplemented with Complete-EDTA-free Protease
618 Inhibitor Cocktail (complete Mini; Sigma Aldrich). Cells were lysed by 30 min incubation on
619 ice and debris were removed by 15 min centrifugation at 2000 g and 4°C. An aliquot of the
620 cleared lysates (50 μL) was kept aside as protein Input. Samples were divided into equal parts
621 (250 μL each) and incubated with 15 μL of magnetic microparticles coated with monoclonal
622 HA or MYC antibodies (MACS purification system, Miltenyi Biotech) at 4°C for 1 hour under
623 rotation (10 rpm). Samples were passed through *μ* Columns (MACS purification system,
624 Miltenyi Biotech). The *μ* Columns were then washed 3 times with 200 μL of lysis buffer and 1
625 time with 100 μL of washing buffer (20 mM Tris-HCl pH 7.5). To elute the immunoprecipitated
626 proteins, 95°C pre-warmed 2x Western blot loading buffer (10% glycerol, 4% SDS, 62.5 mM

627 Tris-HCl pH 6.8, 5% (v/v) 2-β-mercaptoethanol, Bromophenol Blue) was passed through the
628 *μ* Columns. Proteins were analyzed by western blotting or by mass spectrometry.
629 *Endogenous proteins*: The day before immunoprecipitation, magnetic DynaBeads protein G
630 (Invitrogen, ThermoFisher Scientific) were prepared: briefly, 160 μL of magnetic DynaBeads
631 protein G (Invitrogen) were washed three times with lysis buffer (50 mM Tris-HCl pH 7.5, 150
632 mM NaCl, 5 mM EDTA, 1% Triton X-100, 0.5% SDS). The beads were then incubated with 4
633 μg of BSA for 1 h under agitation at room temperature. An aliquot of beads (40 μL) was kept
634 for preclearing step. The remaining beads were incubated either with 6 μg of PKR antibody or
635 control IgG overnight at 4°C under rotation.
636 For the IP: Cells were harvested, washed twice with ice-cold 1× PBS (Gibco®, Life
637 Technologies) and resuspended in 1 mL of lysis buffer (50 mM Tris-HCl pH 7.5, 150 mM
638 NaCl, 5 mM EDTA, 1% Triton X-100, 0.5% SDS) supplemented with Complete-EDTA-free
639 Protease Inhibitor Cocktail (complete Mini; Sigma Aldrich). Cells were lysed by three 15 s
640 sonication steps followed by 30 min incubation on ice and debris were removed by 15 min
641 centrifugation at 16000 g and 4°C. After centrifugation, an aliquot was kept aside as protein
642 Input. Samples were incubated with beads alone for preclearing step for 1 hour at 4°C on wheel.
643 Samples were then put on magnetic racks and the supernatant transferred on new tubes
644 containing either beads coupled to PKR antibody or to control IgG. Samples were incubated on
645 wheel for 3 hours at 4°C. After incubation, samples were put on magnetic racks and beads were
646 washed three times with lysis buffer. After removal of supernatant, beads were eluted with 2x
647 western blot loading buffer and incubated for 10 min at 95°C under agitation. Proteins were
648 analyzed by western blotting.
649
650 **RNase treatment followed by co-IP**

651 *On tagged proteins*: Cells were harvested, washed twice with ice-cold 1× PBS (Gibco®, Life
652 Technologies), and resuspended in 550 µL of lysis buffer (50 mM Tris-HCl pH 7.5, 140 mM
653 NaCl, 1.5 mM $MgCl_2$, 0.1% NP-40), supplemented with Complete-EDTA-free Protease
654 Inhibitor Cocktail (complete Mini; Sigma Aldrich). Cells were lysed by 30 min incubation on
655 ice and debris were removed by 15 min centrifugation at 2000 g and 4°C. Lysate was treated
656 or not with RNase A/T1 mix (ThermoFisher Scientific) and place at 37°C 30min. An aliquot of
657 the cleared lysates (25 µL) was kept aside as protein Input and another aliquot (25 µL) was kept
658 to assess RNase treatment efficiency. Co-IP was led as previously described.
659 Total RNA was extracted using Tri-Reagent Solution (Fisher Scientific; MRC, Inc) according
660 to the manufacturer's instructions. RNA integrity upon treatment was verified on an 1% agarose
661 gel containing ethidium bromide 10 mg/mL (Invitrogen, ThermoFisher Scientific) and revealed
662 under UV on Gel Doc™ EZ system (Bio-Rad).
663
664 **BiFC assay**
665 Experiments were carried out in two different ways. For non-fixed cells, NoDiceΔPKR or
666 HEK293T cells were seeded at the density of 1.2 x 10^5 cells per well in a 24-well plate. After
667 16 hours, cells were transfected with equimolar quantities of each plasmid forming BiFC
668 couples. After 24 hours, cells were infected with SINV at an MOI of 2 and pictures were taken
669 6 hours post-infection using ZOE fluorescent cell imager (Bio-Rad). Proteins were collected
670 with lysis buffer (50 mM Tris-HCl pH 7.5, SDS 0.05%, Triton 1%, 5 mM EDTA, 150 mM
671 NaCl) supplemented with Complete-EDTA-free Protease Inhibitor Cocktail (complete Mini;
672 Sigma Aldrich), and subjected to western blot analysis. For fixed cells, NoDice/ΔPKR cells
673 were seeded at the density of 8.10^4 cells per well in 8-well Millicell® EZ Slides (Merck
674 Millipore), transfected and infected as described previously. At 6 hours post-infection, cells
675 were fixed with 4% formaldehyde and 0.2% glutaraldehyde for 10 min. Cells were then washed

676 with 1× PBS (Gibco®, Life Technologies) and stained with 10 μg/μL DAPI (Invitrogen,
677 ThermoFisher Scientific) in 1× PBS solution (Invitrogen, ThermoFisher Scientific) for 5 min.
678 Fixed cells were mounted on a glass slide with Fluoromount-G mounting media (Southern
679 Biotech). Images were acquired using confocal LSM780 (Zeiss) inverted microscope with an
680 argon laser (514x nm) and with ×40 immersion oil objective. All pictures obtained from BiFC
681 experiments were treated using FigureJ software (NIH).
682
683 **Mass spectrometry analysis**
684 Protein extracts were prepared for mass spectrometry as described in a previous study (Chicois
685 et al., 2018). Each sample was precipitated with 0.1 M ammonium acetate in 100% methanol,
686 and proteins were resuspended in 50 mM ammonium bicarbonate. After a reduction-alkylation
687 step (dithiothreitol 5 mM – iodoacetamide 10 mM), proteins were digested overnight with
688 sequencing-grade porcine trypsin (1:25, w/w, Promega, Fitchburg, MA, USA). The resulting
689 vacuum-dried peptides were resuspended in water containing 0.1% (v/v) formic acid (solvent
690 A). One sixth of the peptide mixtures were analyzed by nanoLC-MS/MS an Easy-nanoLC-1000
691 system coupled to a Q-Exactive Plus mass spectrometer (Thermo-Fisher Scientific, USA)
692 operating in positive mode. Five microliters of each sample were loaded on a C-18 precolumn
693 (75 µm ID × 20 mm nanoViper, 3 μm Acclaim PepMap; Thermo) coupled with the analytical
694 C18 analytical column (75 µm ID × 25 cm nanoViper, 3 μm Acclaim PepMap; Thermo).
695 Peptides were eluted with a 160 min gradient of 0.1% formic acid in acetonitrile at 300 nL/min.
696 The Q-Exactive Plus was operated in data-dependent acquisition mode (DDA) with Xcalibur
697 software (Thermo-Fisher Scientific). Survey MS scans were acquired at a resolution of 70K at
698 200 m/z (mass range 350-1250), with a maximum injection time of 20 ms and an automatic
699 gain control (AGC) set to 3e6. Up to 10 of the most intense multiply charged ions (≥2) were
700 selected for fragmentation with a maximum injection time of 100 ms, an AGC set at 1e5 and a

701 resolution of 17.5K. A dynamic exclusion time of 20 s was applied during the peak selection
702 process.
703
704 **Database search and mass-spectrometry data post-processing**
705 Data were searched against a database containing Human and Viruses UniProtKB sequences
706 with a decoy strategy (GFP, Human and Sindbis Virus SwissProt sequences as well as Semliki
707 Forest Virus SwissProt and TrEMBL sequences (releases from January 2017, 40439
708 sequences)). Peptides were identified with Mascot algorithm (version 2.3, Matrix Science,
709 London, UK) with the following search parameters: carbamidomethylation of cysteine was set
710 as fixed modification; N-terminal protein acetylation, phosphorylation of serine / threonine /
711 tyrosine and oxidation of methionine were set as variable modifications; tryptic specificity with
712 up to three missed cleavages was used. The mass tolerances in MS and MS/MS were set to 10
713 ppm and 0.02 Da respectively, and the instrument configuration was specified as "ESI-Trap".
714 The resulting .dat Mascot files were then imported into Proline v1.4 package
715 (http://proline.profiproteomics.fr/) for post-processing. Proteins were validated with Mascot
716 pretty rank equal to 1, 1% FDR on both peptide spectrum matches (PSM) and protein sets
717 (based on score). The total number of MS/MS fragmentation spectra (Spectral count or SpC)
718 was used for subsequent protein quantification in the different samples.
719
720 **Exploratory and differential expression analysis of LC-MS/MS data**
721 Mass spectrometry data obtained for each sample were stored in a local MongoDB database
722 and subsequently analyzed through a Shiny Application built upon the R/Bioconductor
723 packages msmsEDA (Gregori J, Sanchez A, Villanueva J (2014). msmsEDA: Exploratory Data
724 Analysis of LC-MS/MS data by spectral counts. R/Bioconductor package version 1.22.0) and
725 msmsTests (Gregori J, Sanchez A, Villanueva J (2013). msmsTests: LC-MS/MS Differential

726 Expression Tests. R/Bioconductor package version 1.22.0). Exploratory data analyses of LC-
727 MS/MS data were thus conducted, and differential expression tests were performed using a
728 negative binomial regression model. The p-values were adjusted with FDR control by the
729 Benjamini-Hochberg method and the following criteria were used to define differentially
730 expressed proteins: an adjusted p-value < 0.05, a minimum of 5 SpC in the most abundant
731 condition, and a minimum fold change of 2 (abs(LogFC) > 1).
732
733 **Data availability**
734 The mass spectrometry proteomics data have been deposited to the ProteomeXchange
735 Consortium via the PRIDE (Perez-Riverol et al., 2019) partner repository with the dataset
736 identifier PXD019093 and 10.6019/PXD019093.
737

738 Acknowledgments

739 The authors would like to thank members of the Pfeffer laboratory for discussion, Pr. Bryan
740 Cullen for the kind gift of the HEK293T NoDice and NoDice/ΔPKR cell lines and Dr. Oliver
741 Vugrek for the BiFC plasmids.
742 This work was funded by the European Research Council (ERC-CoG-647455 RegulRNA) and
743 was performed under the framework of the LABEX: ANR-10-LABX-0036_NETRNA and
744 ANR-17-EURE-0023, which benefits from a funding from the state managed by the French
745 National Research Agency as part of the Investments for the future program. This work has
746 also received funding from the People Programme (Marie Curie Actions) of the European
747 Union's Seventh Framework Program (FP7/2007-2013) under REA grant agreement n°
748 PCOFUND-GA-2013-609102, through the PRESTIGE program coordinated by Campus
749 France (to EG), and from the French Minister for Higher Education, Research and Innovation

(PhD contract to MB). The mass spectrometry instrumentation was funded by the University of Strasbourg, IdEx “Equipement mi-lourd” 2015.

Author contributions

SP and ML conceived the project. TCM, ML, EG and SP designed the work. TCM, MB, ML, EG and MM performed the experiments and analyzed the results. PH and JC performed the mass spectrometry analysis. BCWM designed software and analyzed the mass spectrometry results. SP coordinated the work and assured funding. TCM, MB and SP wrote the manuscript with input from the other authors. All authors reviewed and approved the final manuscript.

References

Adiliaghdam, F., Basavappa, M., Saunders, T.L., Harjanto, D., Prior, J.T., Cronkite, D.A., Papavasiliou, N., and Jeffrey, K.L. (2020). A Requirement for Argonaute 4 in Mammalian Antiviral Defense. Cell Rep. *30*, 1690-1701.e4.

Ahmad, S., and Hur, S. (2015). Helicases in Antiviral Immunity: Dual Properties as Sensors and Effectors. Trends Biochem. Sci. *40*, 576–585.

Aktaş, T., Avşar Ilık, İ., Maticzka, D., Bhardwaj, V., Pessoa Rodrigues, C., Mittler, G., Manke, T., Backofen, R., and Akhtar, A. (2017). DHX9 suppresses RNA processing defects originating from the Alu invasion of the human genome. Nature *544*, 115–119.

Backes, S., Langlois, R.A., Schmid, S., Varble, A., Shim, J.V., Sachs, D., and tenOever, B.R. (2014). The Mammalian Response to Virus Infection Is Independent of Small RNA Silencing. Cell Rep. *8*, 114–125.

Bartel, D.P. (2018). Metazoan MicroRNAs. Cell *173*, 20–51.

Berkhout, B. (2018). RNAi-mediated antiviral immunity in mammals. Curr. Opin. Virol. *32*, 9–14.

Bernstein, E., Caudy, A.A., Hammond, S.M., and Hannon, G.J. (2001). Role for a bidentate ribonuclease in the initiation step of RNA interference. Nature *409*, 363–366.

Bogerd, H.P., Skalsky, R.L., Kennedy, E.M., Furuse, Y., Whisnant, A.W., Flores, O., Schultz, K.L.W., Putnam, N., Barrows, N.J., Sherry, B., et al. (2014a). Replication of many human viruses is refractory to inhibition by endogenous cellular microRNAs. J. Virol. *88*, 8065–8076.

Bogerd, H.P., Whisnant, A.W., Kennedy, E.M., Flores, O., and Cullen, B.R. (2014b). Derivation and characterization of Dicer- and microRNA-deficient human cells. RNA *20*, 923–937.

Borden, E.C., Sen, G.C., Uze, G., Silverman, R.H., Ransohoff, R.M., Foster, G.R., and Stark, G.R. (2007). Interferons at age 50: past, current and future impact on biomedicine. Nat. Rev. Drug Discov. *6*, 975–990.

Chakravarthy, S., Sternberg, S.H., Kellenberger, C.A., and Doudna, J.A. (2010). Substrate-Specific Kinetics of Dicer-Catalyzed RNA Processing. J. Mol. Biol. *404*, 392–402.

Chen, E.Y., Tan, C.M., Kou, Y., Duan, Q., Wang, Z., Meirelles, G.V., Clark, N.R., and Ma'ayan, A. (2013). Enrichr: interactive and collaborative HTML5 gene list enrichment analysis tool. BMC Bioinformatics *14*, 128.

Chendrimada, T.P., Gregory, R.I., Kumaraswamy, E., Norman, J., Cooch, N., Nishikura, K., and Shiekhattar, R. (2005). TRBP recruits the Dicer complex to Ago2 for microRNA processing and gene silencing. Nature *436*, 740–744.

Chicois, C., Scheer, H., Garcia, S., Zuber, H., Mutterer, J., Chicher, J., Hammann, P., Gagliardi, D., and Garcia, D. (2018). The UPF1 interactome reveals interaction networks between RNA degradation and translation repression factors in Arabidopsis. Plant J. *96*, 119–132.

Clemens, M.J. (1997). PKR-a protein kinase regulated by double-stranded RNA. Int J Biochem Cell Biol *29*, 945–949.

Clerzius, G., Gélinas, J.-F., Daher, A., Bonnet, M., Meurs, E.F., and Gatignol, A. (2009). ADAR1 interacts with PKR during human immunodeficiency virus infection of lymphocytes and contributes to viral replication. J. Virol. *83*, 10119–10128.

Clerzius, G., Shaw, E., Daher, A., Burugu, S., Gélinas, J.-F., Ear, T., Sinck, L., Routy, J.-P., Mouland, A.J., Patel, R.C., et al. (2013). The PKR activator, PACT, becomes a PKR inhibitor during HIV-1 replication. Retrovirology *10*, 96.

Concordet, J.-P., and Haeussler, M. (2018). CRISPOR: intuitive guide selection for CRISPR/Cas9 genome editing experiments and screens. Nucleic Acids Res. *46*, W242–W245.

809 Cullen, B.R. (2006). Is RNA interference involved in intrinsic antiviral immunity in mammals?
810 Nat Immunol *7*, 563–567.
811 Cullen, B.R. (2017). RNA Interference in Mammals: The Virus Strikes Back. Immunity *46*,
812 970–972.
813 Cullen, B.R., Cherry, S., and tenOever, B.R. (2013). Is RNA Interference a Physiologically
814 Relevant Innate Antiviral Immune Response in Mammals? Cell Host Microbe *14*, 374–
815 378.
816 Daher, A., Laraki, G., Singh, M., Melendez-Peña, C.E., Bannwarth, S., Peters, A.H.F.M.,
817 Meurs, E.F., Braun, R.E., Patel, R.C., and Gatignol, A. (2009). TRBP control of PACT-
818 induced phosphorylation of protein kinase R is reversed by stress. Mol. Cell. Biol. *29*, 254–
819 265.
820 Daniels, S.M., Melendez-Peña, C.E., Scarborough, R.J., Daher, A., Christensen, H.S., El Far,
821 M., Purcell, D.F.J., Lainé, S., and Gatignol, A. (2009). Characterization of the TRBP
822 domain required for dicer interaction and function in RNA interference. BMC Mol. Biol.
823 *10*, 38.
824 Donaszi-Ivanov, A., Mohorianu, I., Dalmay, T., and Powell, P.P. (2013). Small RNA Analysis
825 in Sindbis Virus Infected Human HEK293 Cells. PLoS ONE *8*, e84070.
826 Doyle, M., Badertscher, L., Jaskiewicz, L., Güttinger, S., Jurado, S., Hugenschmidt, T., Kutay,
827 U., and Filipowicz, W. (2013). The double-stranded RNA binding domain of human Dicer
828 functions as a nuclear localization signal. RNA N. Y. N *19*, 1238–1252.
829 Elde, N.C., Child, S.J., Geballe, A.P., and Malik, H.S. (2009). Protein kinase R reveals an
830 evolutionary model for defeating viral mimicry. Nature *457*, 485–489.
831 Fairman-Williams, M.E., Guenther, U.-P., and Jankowsky, E. (2010). SF1 and SF2 helicases:
832 family matters. Curr. Opin. Struct. Biol. *20*, 313–324.
833 Fros, J.J., and Pijlman, G.P. (2016). Alphavirus Infection: Host Cell Shut-Off and Inhibition of
834 Antiviral Responses. Viruses *8*, 166.
835 Fujii, R., Okamoto, M., Aratani, S., Oishi, T., Ohshima, T., Taira, K., Baba, M., Fukamizu, A.,
836 and Nakajima, T. (2001). A Role of RNA Helicase A in cis-Acting Transactivation
837 Response Element-mediated Transcriptional Regulation of Human Immunodeficiency
838 Virus Type 1. J. Biol. Chem. *276*, 5445–5451.
839 Gal-Ben-Ari, S., Barrera, I., Ehrlich, M., and Rosenblum, K. (2018). PKR: A Kinase to
840 Remember. Front. Mol. Neurosci. *11*, 480.
841 García, M.A., Meurs, E.F., and Esteban, M. (2007). The dsRNA protein kinase PKR: Virus and
842 cell control. Biochimie *89*, 799–811.
843 Girardi, E., Chane-Woon-Ming, B., Messmer, M., Kaukinen, P., and Pfeffer, S. (2013).
844 Identification of RNase L-dependent, 3'-end-modified, viral small RNAs in Sindbis virus-
845 infected mammalian cells. MBio *4*, e00698-00613.
846 Girardi, E., Lefèvre, M., Chane-Woon-Ming, B., Paro, S., Claydon, B., Imler, J.-L., Meignin,
847 C., and Pfeffer, S. (2015). Cross-species comparative analysis of Dicer proteins during
848 Sindbis virus infection. Sci. Rep. *5*, 10693.
849 Griffin, D. (2007). Alphaviruses, p 1023–1067. Fields Virol. 5th Ed Lippincott Williams
850 Wilkins Phila. PA.
851 Guo, Z., Li, Y., and Ding, S.-W. (2019). Small RNA-based antimicrobial immunity. Nat. Rev.
852 Immunol. *19*, 31–44.
853 Haase, A.D., Jaskiewicz, L., Zhang, H., Laine, S., Sack, R., Gatignol, A., and Filipowicz, W.
854 (2005). TRBP, a regulator of cellular PKR and HIV-1 virus expression, interacts with Dicer
855 and functions in RNA silencing. EMBO Rep *6*, 961–967.
856 Herbert, A., Alfken, J., Kim, Y.G., Mian, I.S., Nishikura, K., and Rich, A. (1997). A Z-DNA
857 binding domain present in the human editing enzyme, double-stranded RNA adenosine
858 deaminase. Proc. Natl. Acad. Sci. U. S. A. *94*, 8421–8426.

859 Heyam, A., Lagos, D., and Plevin, M. (2015). Dissecting the roles of TRBP and PACT in
860 double-stranded RNA recognition and processing of noncoding RNAs. WIREs RNA *6*,
861 271–289.
862 Hutvágner, G., McLachlan, J., Pasquinelli, A.E., Balint, E., Tuschl, T., and Zamore, P.D.
863 (2001). A cellular function for the RNA-interference enzyme Dicer in the maturation of
864 the let-7 small temporal RNA. Science *293*, 834–838.
865 Iizasa, H., Wulff, B.-E., Alla, N.R., Maragkakis, M., Megraw, M., Hatzigeorgiou, A., Iwakiri,
866 D., Takada, K., Wiedmer, A., Showe, L., et al. (2010). Editing of Epstein-Barr virus-
867 encoded BART6 microRNAs controls their dicer targeting and consequently affects viral
868 latency. J. Biol. Chem. *285*, 33358–33370.
869 Ivashkiv, L.B., and Donlin, L.T. (2014). Regulation of type I interferon responses. Nat. Rev.
870 Immunol. *14*, 36–49.
871 Kennedy, E.M., Whisnant, A.W., Kornepati, A.V.R., Marshall, J.B., Bogerd, H.P., and Cullen,
872 B.R. (2015). Production of functional small interfering RNAs by an amino-terminal
873 deletion mutant of human Dicer. Proc. Natl. Acad. Sci. *112*, E6945–E6954.
874 Kim, Y., Lee, J.H., Park, J.-E., Cho, J., Yi, H., and Kim, V.N. (2014). PKR is activated by
875 cellular dsRNAs during mitosis and acts as a mitotic regulator. Genes Dev. *28*, 1310–1322.
876 Kok, K.H., Ng, M.H., Ching, Y.P., and Jin, D.Y. (2007). Human TRBP and PACT Directly
877 Interact with Each Other and Associate with Dicer to Facilitate the Production of Small
878 Interfering RNA. J Biol Chem *282*, 17649–17657.
879 Kok, K.-H., Lui, P.-Y., Ng, M.-H.J., Siu, K.-L., Au, S.W.N., and Jin, D.-Y. (2011). The Double-
880 Stranded RNA-Binding Protein PACT Functions as a Cellular Activator of RIG-I to
881 Facilitate Innate Antiviral Response. Cell Host Microbe *9*, 299–309.
882 Kuleshov, M.V., Jones, M.R., Rouillard, A.D., Fernandez, N.F., Duan, Q., Wang, Z., Koplev,
883 S., Jenkins, S.L., Jagodnik, K.M., Lachmann, A., et al. (2016). Enrichr: a comprehensive
884 gene set enrichment analysis web server 2016 update. Nucleic Acids Res. *44*, W90-97.
885 Lambert, M., Pépin, G., Peralta-Zaragoza, O., Matusiak, R., Ly, S., Landry, P., and Provost, P.
886 (2016). TWEAK Negatively Regulates Human Dicer. Non-Coding RNA *2*.
887 Lee, Y., Hur, I., Park, S.Y., Kim, Y.K., Suh, M.R., and Kim, V.N. (2006). The role of PACT
888 in the RNA silencing pathway. Embo J *25*, 522–532.
889 Lemaire, P.A., Anderson, E., Lary, J., and Cole, J.L. (2008). Mechanism of PKR Activation by
890 dsRNA. J. Mol. Biol. *381*, 351–360.
891 Lepur, A., Kovačević, L., Belužić, R., and Vugrek, O. (2016). Combining unique multiplex
892 gateway cloning and bimolecular fluorescence complementation (BiFC) for high-
893 throughput screening of protein–protein interactions. J. Biomol. Screen. *21*, 1100–1111.
894 Li, J., Tang, H., Mullen, T.M., Westberg, C., Reddy, T.R., Rose, D.W., and Wong-Staal, F.
895 (1999). A role for RNA helicase A in post-transcriptional regulation of HIV type 1. Proc.
896 Natl. Acad. Sci. U. S. A. *96*, 709–714.
897 Li, Y., Lu, J., Han, Y., Fan, X., and Ding, S.-W. (2013). RNA interference functions as an
898 antiviral immunity mechanism in mammals. Science *342*, 231–234.
899 Li, Y., Basavappa, M., Lu, J., Dong, S., Cronkite, D.A., Prior, J.T., Reinecker, H.-C., Hertzog,
900 P., Han, Y., Li, W.-X., et al. (2016). Induction and suppression of antiviral RNA
901 interference by influenza A virus in mammalian cells. Nat. Microbiol. *2*, 16250.
902 Li, Z., Wolff, K.C., and Samuel, C.E. (2010). RNA adenosine deaminase ADAR1 deficiency
903 leads to increased activation of protein kinase PKR and reduced vesicular stomatitis virus
904 growth following interferon treatment. Virology *396*, 316–322.
905 Lui, P.-Y., Wong, L.-Y.R., Ho, T.-H., Au, S.W.N., Chan, C.-P., Kok, K.-H., and Jin, D.-Y.
906 (2017). PACT Facilitates RNA-Induced Activation of MDA5 by Promoting MDA5
907 Oligomerization. J. Immunol. *199*, 1846–1855.

908 Maillard, P.V., Ciaudo, C., Marchais, A., Li, Y., Jay, F., Ding, S.W., and Voinnet, O. (2013).
909 Antiviral RNA interference in mammalian cells. Science *342*, 235–238.
910 Maillard, P.V., Veen, A.G.V. der, Deddouche-Grass, S., Rogers, N.C., Merits, A., and Sousa,
911 C.R. e (2016). Inactivation of the type I interferon pathway reveals long double-stranded
912 RNA-mediated RNA interference in mammalian cells. EMBO J. *35*, 2505–2518.
913 Maillard, P.V., van der Veen, A.G., Poirier, E.Z., and Reis e Sousa, C. (2019). Slicing and
914 dicing viruses: antiviral RNA interference in mammals. EMBO J. *38*.
915 Meister, G., and Tuschl, T. (2004). Mechanisms of gene silencing by double-stranded RNA.
916 Nature *431*, 343–349.
917 Meister, G., Landthaler, M., Peters, L., Chen, P.Y., Urlaub, H., Lührmann, R., and Tuschl, T.
918 (2005). Identification of novel argonaute-associated proteins. Curr. Biol. CB *15*, 2149–
919 2155.
920 Mittelstadt, M., Frump, A., Khuu, T., Fowlkes, V., Handy, I., Patel, C.V., and Patel, R.C.
921 (2008). Interaction of human tRNA-dihydrouridine synthase-2 with interferon-induced
922 protein kinase PKR. Nucleic Acids Res. *36*, 998–1008.
923 Nakamura, T., Kunz, R.C., Zhang, C., Kimura, T., Yuan, C.L., Baccaro, B., Namiki, Y., Gygi,
924 S.P., and Hotamisligil, G.S. (2015). A Critical Role for PKR Complexes with TRBP in
925 Immunometabolic Regulation and eIF2α Phosphorylation in Obesity. Cell Rep. *11*, 295–
926 307.
927 Ota, H., Sakurai, M., Gupta, R., Valente, L., Wulff, B.-E., Ariyoshi, K., Iizasa, H., Davuluri,
928 R.V., and Nishikura, K. (2013). ADAR1 forms a complex with Dicer to promote
929 microRNA processing and RNA-induced gene silencing. Cell *153*, 575–589.
930 Parameswaran, P., Sklan, E., Wilkins, C., Burgon, T., Samuel, M.A., Lu, R., Ansel, K.M.,
931 Heissmeyer, V., Einav, S., Jackson, W., et al. (2010). Six RNA viruses and forty-one hosts:
932 viral small RNAs and modulation of small RNA repertoires in vertebrate and invertebrate
933 systems. PLoS Pathog *6*, e1000764.
934 Park, H., Davies, M.V., Langland, J.O., Chang, H.W., Nam, Y.S., Tartaglia, J., Paoletti, E.,
935 Jacobs, B.L., Kaufman, R.J., and Venkatesan, S. (1994). TAR RNA-binding protein is an
936 inhibitor of the interferon-induced protein kinase PKR. Proc. Natl. Acad. Sci. U. S. A. *91*,
937 4713–4717.
938 Patel, C.V., Handy, I., Goldsmith, T., and Patel, R.C. (2000). PACT, a Stress-modulated
939 Cellular Activator of Interferon-induced Double-stranded RNA-activated Protein Kinase,
940 PKR. J. Biol. Chem. *275*, 37993–37998.
941 Perez-Riverol, Y., Csordas, A., Bai, J., Bernal-Llinares, M., Hewapathirana, S., Kundu, D.J.,
942 Inuganti, A., Griss, J., Mayer, G., Eisenacher, M., et al. (2019). The PRIDE database and
943 related tools and resources in 2019: improving support for quantification data. Nucleic
944 Acids Res. *47*, D442–D450.
945 Pfaller, C.K., Li, Z., George, C.X., and Samuel, C.E. (2011). Protein kinase PKR and RNA
946 adenosine deaminase ADAR1: new roles for old players as modulators of the interferon
947 response. Curr. Opin. Immunol. *23*, 573–582.
948 Qiu, Y., Xu, Y., Zhang, Y., Zhou, H., Deng, Y.-Q., Li, X.-F., Miao, M., Zhang, Q., Zhong, B.,
949 Hu, Y., et al. (2017). Human Virus-Derived Small RNAs Can Confer Antiviral Immunity
950 in Mammals. Immunity *46*, 992-1004.e5.
951 Qiu, Y., Xu, Y.-P., Wang, M., Miao, M., Zhou, H., Xu, J., Kong, J., Zheng, D., Li, R.-T., and
952 Zhang, R.-R. (2020). Flavivirus induces and antagonizes antiviral RNA interference in both
953 mammals and mosquitoes. Sci. Adv. *6*, eaax7989.
954 Robb, G.B., and Rana, T.M. (2007). RNA helicase A interacts with RISC in human cells and
955 functions in RISC loading. Mol. Cell *26*, 523–537.

Roy, B.B., Hu, J., Guo, X., Russell, R.S., Guo, F., Kleiman, L., and Liang, C. (2006). Association of RNA helicase a with human immunodeficiency virus type 1 particles. J. Biol. Chem. *281*, 12625–12635.

Ryman, K.D., White, L.J., Johnston, R.E., and Klimstra, W.B. (2002). Effects of PKR/RNase L-Dependent and Alternative Antiviral Pathways on Alphavirus Replication and Pathogenesis. Viral Immunol. *15*, 53–76.

Sadler, A.J., Latchoumanin, O., Hawkes, D., Mak, J., and Williams, B.R.G. (2009). An Antiviral Response Directed by PKR Phosphorylation of the RNA Helicase A. PLoS Pathog. *5*, e1000311.

Samuel, C.E. (2011). Adenosine deaminases acting on RNA (ADARs) are both antiviral and proviral. Virology *411*, 180–193.

Schoggins, J.W., Wilson, S.J., Panis, M., Murphy, M.Y., Jones, C.T., Bieniasz, P., and Rice, C.M. (2011). A diverse range of gene products are effectors of the type I interferon antiviral response. Nature *472*, 481–485.

Schuster, S., Overheul, G.J., Bauer, L., van Kuppeveld, F.J.M., and van Rij, R.P. (2019). No evidence for viral small RNA production and antiviral function of Argonaute 2 in human cells. Sci. Rep. *9*, 1–11.

Singh, M., Castillo, D., Patel, C.V., and Patel, R.C. (2011). Stress-induced phosphorylation of PACT reduces its interaction with TRBP and leads to PKR activation. Biochemistry *50*, 4550–4560.

Takahashi, T., and Ui-Tei, K. (2020). Mutual Regulation of RNA Silencing and the IFN Response as an Antiviral Defense System in Mammalian Cells. Int. J. Mol. Sci. *21*, 1348.

Takahashi, T., Nakano, Y., Onomoto, K., Murakami, F., Komori, C., Suzuki, Y., Yoneyama, M., and Ui-Tei, K. (2018a). LGP2 virus sensor regulates gene expression network mediated by TRBP-bound microRNAs. Nucleic Acids Res. *46*, 9134–9147.

Takahashi, T., Nakano, Y., Onomoto, K., Yoneyama, M., and Ui-Tei, K. (2018b). Virus Sensor RIG-I Represses RNA Interference by Interacting with TRBP through LGP2 in Mammalian Cells. Genes *9*, 511.

tenOever, B.R. (2016). The Evolution of Antiviral Defense Systems. Cell Host Microbe *19*, 142–149.

Tsai, K., Courtney, D.G., Kennedy, E.M., and Cullen, B.R. (2018). Influenza A virus-derived siRNAs increase in the absence of NS1 yet fail to inhibit virus replication. RNA N. Y. N.

van der Veen, A.G., Maillard, P.V., Schmidt, J.M., Lee, S.A., Deddouche-Grass, S., Borg, A., Kjær, S., Snijders, A.P., and Reis e Sousa, C. (2018). The RIG-I-like receptor LGP2 inhibits Dicer-dependent processing of long double-stranded RNA and blocks RNA interference in mammalian cells. EMBO J. *37*, e97479.

Wienholds, E., Koudijs, M.J., Van Eeden, F.J., Cuppen, E., and Plasterk, R.H. (2003). The microRNA-producing enzyme Dicer1 is essential for zebrafish development. Nat Genet 217–218.

Williams, B.R. (1999). PKR; a sentinel kinase for cellular stress. Oncogene *18*, 6112–6120.

Yang, W., Chendrimada, T.P., Wang, Q., Higuchi, M., Seeburg, P.H., Shiekhattar, R., and Nishikura, K. (2006). Modulation of microRNA processing and expression through RNA editing by ADAR deaminases. Nat Struct Mol Biol *13*, 13–21.

1001 ## Figure legends

1002 **Figure 1. Analysis of SINV infection in HEK293T cells and characterization of**
1003 **FHA:DICER WT cell lines.**

1004 **A.** GFP fluorescent microscopy pictures of HEK293T, NoDice FHA:ctrl #1 and FHA:DICER
1005 cell lines infected (polyclonal and two clones, #4 and #17) with SINV-GFP at an MOI of 0.02
1006 for 24 h. The left panel corresponds to GFP signal from infected cells and the right panel to a
1007 merge picture of GFP signal and brightfield. Pictures were taken with a 5x magnification. hpi:
1008 hours post-infection. **B.** Western blot analysis of DICER (DICER and HA) and GFP expression
1009 in SINV-GFP-infected HEK293T, NoDice FHA:ctrl #1 and FHA:DICER cell lines shown in
1010 **A**. Gamma-Tubulin was used as loading control. **C.** Mean (+/- SEM) of SINV-GFP viral titers
1011 in the same cell lines as in **A** infected at an MOI of 0.02 for 24 h (n = 3) from plaque assay
1012 quantification. ns: non-significant, ordinary one-way ANOVA test with Bonferroni correction.
1013 **D.** Western blot analysis of DICER (DICER and HA) and AGO2 expression in HEK293T,
1014 NoDice FHA:ctrl #1 and FHA:DICER cell lines. Gamma-Tubulin was used as loading control.
1015

1016 **Figure 2. LC-MS/MS analysis of DICER interactome during SINV infection.**

1017 **A.** Volcano plot for differentially expressed proteins (DEPs) between HA IP and CTL IP in
1018 FHA:DICER mock-infected cells. Each protein is marked as a dot; proteins that are
1019 significantly up-regulated in HA IP are shown in red, up-regulated proteins in CTL IP are
1020 shown in blue, and non-significant proteins are in black. The horizontal line denotes a p-value
1021 of 0.05 and the vertical lines the Log2 fold change cutoff (-1 and 1). DICER and its cofactors
1022 (TRBP, PACT, AGO2) are highlighted in yellow. **B.** Volcano plot for DEPs between SINV-
1023 GFP (MOI of 2, 6 hpi) and mock fractions of HA IP in FHA:DICER cells. Same colour code
1024 and thresholds as in A have been applied. Proteins that are discussed in the text are highlighted
1025 in yellow and SINV proteins in purple. **C.** Gene Ontology (GO) term enrichment of proteins

1026 up-regulated in SINV-GFP fraction of HA IP using Enrichr software (Chen et al., 2013;
1027 Kuleshov et al., 2016). The graph displays the GO term hierarchy within the "biological
1028 process" branch sorted by p-value ranking computed from the Fisher exact test. The length of
1029 each bar represents the significance of that specific term. In addition, the brighter the colour is,
1030 the more significant that term is. Viral proteins have been excluded for this analysis. **D.**
1031 Summary of the differential expression analysis of SINV-GFP vs mock fractions from HA IP
1032 in FHA:DICER cells. The analysis has been performed using a generalized linear model of a
1033 negative-binomial distribution and p-values were corrected for multiple testing using the
1034 Benjamini-Hochberg method.
1035
1036 **Figure 3. Confirmation of LC-MS/MS analysis by co-IP and BiFC.**
1037 **A.** Western blot analysis of HA co-IP in mock or SINV-GFP-infected (MOI of 2, 6 hpi)
1038 FHA:DICER WT #4 cells. Proteins associated to FHA:DICER were revealed by using
1039 antibodies targeting endogenous ADAR-1, PKR, TRBP, DHX9 or PACT proteins. In parallel,
1040 an HA antibody was used to verify the IP efficiency and GFP antibody was used to verify the
1041 infection. Ponceau was used as loading control. **B.** Western blot analysis of HA co-IP in mock
1042 or SINV-GFP-infected (MOI of 2, 6 hpi) FHA:DICER WT #4 cells. The lysate was treated or
1043 not with RNase A/T1. Proteins associated to FHA:DICER were revealed by using antibodies
1044 targeting endogenous DHX9, p-PKR, PKR, TRBP, or PACT proteins. In parallel, an HA
1045 antibody was used to verify the IP efficiency and GFP antibody was used to verify the infection.
1046 Ponceau was used as loading control. The arrow points to the expected size of the FHA:DICER
1047 protein and the asterisks correspond to aspecific bands. **C.** Western blot analysis to validate the
1048 interaction of PKR with DICER (upper panel) and PACT (lower panel) in mock or SINV-GFP-
1049 infected HEK293T cells. Immunoprecipitated proteins obtained from PKR pulldowns were
1050 compared to IgG pulldowns to verify the specificity of the assay. **D.** Interactions between

1051 DICER and TRBP, PACT or PKR were visualized by BiFC. Plasmids expressing $^{N-}$
1052 ^{ter}Venus:DICER and TRBP:, PACT: or PKR:Venus^{C-ter} were co-transfected in NoDice/ΔPKR
1053 cells for 24 h and cells were either infected with SINV at an MOI of 2 for 6 h or not. The
1054 different combinations are indicated on the left side. Reconstitution of Venus (BiFC) signal was
1055 observed under epifluorescence microscope. For each condition, the left panel corresponds to
1056 Venus signal and the right panel to the corresponding brightfield pictures. Scale bar: 100 μm.
1057 hpi: hours post-infection. **E.** BiFC experiment on fixed NoDice/ΔPKR cells treated as in D.
1058 After fixation, cells were stained with DAPI and observed under confocal microscope. Only a
1059 merge picture of BiFC and DAPI signals of SINV-infected cells is shown here. A higher
1060 magnification of picture showing cytoplasmic localization of the interaction represented by a
1061 red square is shown in the bottom left corner. Scale bar: 20 μm and 10 μm.
1062
1063 **Figure 4. Confirmation of DICER interactome upon SINV infection in HCT116 KI-**
1064 **DICER cells.**
1065 **A.** Western blot analysis of DICER, AGO2, PKR and TRBP expression in HEK293T, HCT116
1066 and HCT116 KI-DICER cell lines. Gamma-Tubulin and ponceau were used as loading control.
1067 **B**. GFP fluorescent microscopy pictures of HEK293T, HCT116 and HCT116 KI-DICER cell
1068 lines infected with SINV-GFP at an MOI of 0.02, 0.1 and 1 for 24 h. The left panel corresponds
1069 to GFP signal from infected cells and the right panel to a merge picture of GFP signal and
1070 brightfield. Pictures were taken with a 5x magnification. **C**. miR-16 expression analyzed by
1071 northern blot in in the same cell lines as in B. Expression of snRNA U6 was used as loading
1072 control. **D.** Western blot analysis of HA co-IP in mock or SINV-GFP-infected (MOI of 0.1, 24
1073 hpi) HCT116 KI-DICER cells. Proteins associated to FHA-GFP:DICER were revealed by using
1074 antibodies targeting endogenous DHX9, p-PKR, PKR, PACT or TRBP proteins. In parallel, an

1075 HA antibody was used to verify the IP efficiency and GFP antibody was used to verify the
1076 infection. Ponceau was used as loading control.
1077
1078 **Figure 5. Identification of DICER domains involved in DICER-PKR interaction.**
1079 **A.** Schematic representation of Human DICER proteins used in this study. The different
1080 conserved domains are shown in colored boxes. DUF283: Domain of Unknown Function; PAZ:
1081 PIWI ARGONAUTE ZWILLE domain; dsRBD: dsRNA-binding domain. hDICER WT is the
1082 full-length protein. hDICER N1 is deleted of the first N-terminal 495 amino acids. hDICER N3
1083 is wholly deleted of the helicase domain. hDICER Hel. is the whole DICER's helicase domain.
1084 hDICER ΔdsRBD is deleted of the C-terminal dsRBD. **B.** Western blot analysis of HA co-IP
1085 in mock NoDice 2.20 cells transfected with different versions of FHA:DICER proteins.
1086 Efficiency of immunoprecipitation was assessed using anti-HA and anti-DICER antibodies and
1087 co-IPs of TRBP, PKR and PACT were examined using appropriate antibodies. Expression of
1088 GFP in INPUT fraction was visualized as control of SINV-GFP infection. Ponceau staining of
1089 membranes is used as loading control. **C.** Western blot analysis of HA co-IP in NoDice 2.20
1090 cells transfected with different versions of FHA:DICER proteins and infected with SINV-GFP
1091 (MOI of 2, 6 hpi). Efficiency of immunoprecipitation was assessed using an anti- Flag antibody
1092 and co-IPs of PKR, TRBP, p-PKR and PACT were examined using appropriate antibodies.
1093 Expression of GFP in INPUT fraction was visualized as control of SINV-GFP infection.
1094 Ponceau staining of membranes is used as loading control. **D.** Plasmids expressing the different
1095 versions of DICER proteins fused to the N-terminal part of Venus and PKR:Venus$^{C\text{-}ter}$ plasmid
1096 were co-transfected in NoDice/ΔPKR cells. Cells were treated as in Fig. 3D. The different
1097 combinations are noted on the left side. The fluorescent signal was observed using an
1098 epifluorescence microscope. For each condition, the left panel corresponds to Venus signal and

1099 the right panel to the corresponding brightfield pictures. Scale bar: 100 μm. hpi: hours post-
1100 infection.
1101
1102 **Figure 6. Analysis of the importance of Dicer helicase domain on SINV-GFP infection in**
1103 **FHA:DICER mutant stable cell lines.**
1104 **A.** Expression of DICER (DICER, HA), TRBP and AGO2 was analysed by western blot in
1105 HEK293T, NoDice FHA:ctrl #1, FHA:DICER WT #4 and FHA:DICER N1 #6 cell lines.
1106 Gamma-Tubulin was used as loading control. **B.** Northern blot analysis of miR-16 expression
1107 in the same samples as in A. Expression of snRNA U6 was used as loading control. **C.**
1108 Representative GFP fluorescent microscopy images of HEK293T, FHA:DICER WT #4 and
1109 FHA:DICER N1 #6 cell lines infected with SINV-GFP at an MOI of 0.02 for 24 h. The left
1110 panel corresponds to GFP signal and the right panel to a merge picture of GFP signal and
1111 brightfield. Pictures were taken with a 5x magnification. hpi: hours post-infection. **D.** Western
1112 blot analysis of DICER (DICER and HA), AGO2, PKR, and GFP expression in SINV-GFP-
1113 infected cells in the same condition as in C. Gamma-Tubulin was used as loading control. The
1114 asterisk correspond to aspecific bands **E.** Mean (+/- SEM) of SINV-GFP viral titers fold change
1115 over HEK293T cells in HEK293T, NoDice 2.20, FHA:DICER WT #4 and FHA:DICER
1116 mutants cell lines infected at an MOI of 0.02 for 24 h (n = 3) from plaque assay quantification.
1117 * $p < 0.05$, ns: non-significant, ordinary one-way ANOVA test with Bonferroni correction.
1118

1119 # Supplementary material

1120

1121 **Supplementary figure legends**

1122 **Figure S1. Analysis of SINV-GFP infection in FHA:DICER cell lines at different MOI**
1123 **and time points.**

1124 **A.** miR-16 expression analyzed by northern blot in HEK293T, NoDice FHA:ctrl #1 and
1125 FHA:DICER WT #4 cell lines**.** Expression of snRNA U6 was used as loading control. **B.**
1126 Representative GFP pictures of HEK293T, NoDice 2.20, NoDice 4.25, NoDice FHA:ctrl #1
1127 and NoDice FHA:ctrl #2 cells infected with SINV-GFP at an MOI of 0.02 for 24h. The left
1128 panel corresponds to GFP signal and the right panel to a merge of GFP signal and the
1129 corresponding brightfield. Pictures were taken with a 5x magnification. hpi: hours post-
1130 infection. **C.** Mean (+/- SEM) of SINV-GFP viral titers in cells infected at an MOI of 0.02 for
1131 24 h (n=3) from plaque assay quantification. * $p < 0.05$, ns: non-significant, ordinary one-way
1132 ANOVA test with Bonferroni correction. **D**. Western blot analysis of DICER, AGO2 and GFP
1133 expression in SINV-GFP-infected cells shown in B. Gamma-Tubulin was used as loading
1134 control.

1135

1136 **Figure S2. LC-MS/MS analysis of DICER interactome during SFV infection.**

1137 **A.** Volcano plot for differentially expressed proteins (DEPs) between HA IP and CTL IP in
1138 FHA:DICER mock-infected cells. Each protein is marked as a dot; proteins that are
1139 significantly up-regulated in HA IP are shown in red, up-regulated proteins in CTL IP are
1140 shown in blue, and non-significant proteins are in black. The horizontal line denotes a p-value
1141 of 0.05 and the vertical lines the Log2 fold change cutoff (-1 and 1). DICER and its cofactors
1142 (TRBP, PACT, AGO2) are highlighted in yellow. **B.** Left panel: Volcano plot for DEPs
1143 between SFV (MOI of 2, 6 hpi) and mock fractions of HA IP in FHA:DICER cells. Same colour

1144 code and thresholds as in A were applied. Proteins that are discussed in the text are highlighted
1145 in yellow and SFV proteins in purple. **C.** Summary of the differential expression analysis of
1146 SFV vs mock fractions from HA IP in FHA:DICER cells. The analysis has been performed
1147 using a generalized linear model of a negative-binomial distribution and p-values were
1148 corrected for multiple testing using the Benjamini-Hochberg method.
1149
1150 **Figure S3. Confirmation of LC-MS/MS analysis by co-IP and BiFC controls.**
1151 **A.** FHA:DICER WT #4 cells were infected with SINV-GFP at an MOI of 0.02 for 24 h and a
1152 HA co-IP was performed. Eluted proteins were resolved by western blot and IP efficiency was
1153 assessed using an HA antibody. In parallel, co-IPed proteins were visualized using appropriate
1154 antibodies. GFP antibody was used to verify the infection and Ponceau staining serves as
1155 loading control. **B.** 1% Agarose gel analysis of RNA extracted from INPUT of the co-IP in Fig.
1156 3B. Ribosomal RNA integrity was compared to a control HEK293T cell line. RNAs were
1157 revealed using ethidium bromide under UV. **C.** Schematic representation of Human DICER
1158 proteins used for BiFC positive and negative controls. The different conserved domains are
1159 shown in colored boxes. DUF283: Domain of Unknown Function; PAZ: PIWI ARGONAUTE
1160 ZWILLE domain; dsRBD: dsRNA-binding domain. hDICER WT is the full-length protein.
1161 hDICER N1 is deleted of the first N-terminal 495 amino acids. **D.** Expression of BiFC plasmids
1162 was assessed by western blot. DICER proteins (WT and N1) and PKR were visualized using
1163 antibodies targeting endogenous proteins, whereas TRBP and PACT were detected using GFP
1164 antibody. Antibody targeting the SINV coat protein (CP) was used as infection control. Ponceau
1165 staining was used as loading control. **E.** Positive and negative BiFC controls on fixed
1166 NoDice/ΔPKR cells. After co-transfection, cells were infected with SINV at an MOI of 2 for 6
1167 h and fixed. After fixation, cells were stained with DAPI and observed under confocal
1168 microscope. Merge pictures of BiFC and DAPI signals of SINV-infected cells are shown. A

1169 higher magnification of images showing the interaction represented by a red square is shown
1170 in the bottom left corner. Scale bar: 20 μm and 10 μm. **F.** Expression of BiFC plasmids was
1171 assessed by western blot. DICER, PKR, TRBP and PACT were detected using GFP antibody.
1172 Antibody targeting the SINV coat protein (CP) was used as infection control. Gamma-Tubulin
1173 was used as loading control. The asterisk corresponds to an aspecific band. **G.** Interactions
1174 between DICER and TRBP, PACT or PKR were visualized by BiFC. Plasmids expressing $^{N-}$
1175 ^{ter}Venus:DICER and TRBP:, PACT: or PKR:Venus^{C-ter} were co-transfected in HEK293T cells
1176 for 24 h and cells were either infected with SINV at an MOI of 2 for 6 h or not. The different
1177 combinations are indicated on the left side. Reconstitution of Venus (BiFC) signal was observed
1178 under epifluorescence microscope. For each condition, the left panel corresponds to Venus
1179 signal and the right panel to the corresponding brightfield pictures. Scale bar: 100 μm.
1180
1181 **Figure S4. Confirmation of DICER interactome upon SINV infection in HCT116 KI-**
1182 **DICER cells.**
1183 **A.** Schematic representation of DICER WT and Flag-HA(FHA)-GFP kocked-in (KI) alleles.
1184 FHA sequence is in purple, GFP in green, DICER 5'UTR in orange and DICER coding region
1185 in yellow. The gRNA used to generate the KI was designed to target the first coding exon of
1186 DICER gene. **B.** PCR on genomic DNA extracted from WT and KI cells. **C.** An oligo outside
1187 the homologous recombination region and an oligo within the GFP tag were used to verify the
1188 presence of a 1040bp amplicon in HCT116 KI-DICER clone. Sequencing results corresponding
1189 to this region are shown. **D.** Western blot analysis of DICER, p-PKR, PKR and p-eIF2α
1190 expression in mock or SINVGFP-infected HEK293T and HCT116 KI-DICER cell lines at an
1191 MOI of 2 for 6h or 16h and 0.02 for 24h. GFP antibody was used to verify the infection. Ponceau
1192 and gamma-Tubulin were used as loading control.
1193

1194 **Figure S5. Interaction analysis between the different versions of DICER and TRBP or**
1195 **PACT using BiFC assay.**
1196 NoDice/ΔPKR cells were co-transfected for 24 h with plasmids expressing the different
1197 versions of DICER proteins fused to the N-terminal part of Venus and either TRBP:Venus$^{C\text{-}ter}$
1198 (**A**) or PACT:Venus$^{C\text{-}ter}$ (**B**). Cells were then infected with SINV at an MOI of 2 for 6 h and
1199 Venus signal was observed under epifluorescence microscope. The left panel corresponds to
1200 Venus signal and the right panel to the corresponding brightfield picture. Pictures were taken
1201 with a 5x magnification. hpi: hours post-infection. Scale bar: 100 µm.
1202
1203 **Figure S6. Analysis of the importance of Dicer helicase domain on SINV-GFP infection in**
1204 **FHA:DICER mutant stable cell lines.**
1205 **A**. Northern blot analysis of miR-16 expression in HEK293T, NoDice 2.20, NoDice FHA:ctrl
1206 #2, FHA:DICER WT polyclonal, FHA:DICER N1 #6, FHA:DICER Hel. #2.6, and
1207 FHA:DICER N3 #2.13. Expression of snRNA U6 was used as loading control. **B.**
1208 Representative GFP fluorescent microscopy images of HEK293T, NoDice 2.20, FHA:DICER
1209 mutants cell lines infected with SINV-GFP at an MOI of 0.02 for 24 h. The left panel
1210 corresponds to GFP signal and the right panel to a merge picture of GFP signal and brightfield.
1211 Pictures were taken with a 5x magnification. hpi: hours post-infection. **C**. Mean (+/- SEM) of
1212 SINV-GFP viral titers over FHA:DICER WT #4 cells in FHA:DICER N1 #6, FHA:DICER N3
1213 #2.13, NoDice FHA:ctrl #2 and NoDice 2.20 cell lines infected at an MOI of 0.02 for 24 h (n
1214 = 3) from plaque assay quantification. *** $p < 0.001$, ns: non-significant, ordinary one-way
1215 ANOVA test with Bonferroni correction.
1216
1217 **Supplementary tables**

1218 **Supp. Table 1:** Top 100 proteins that are differentially immunoprecipitated in mock-infected
1219 FHA:DICER cells by the HA and Myc (CTL) antibodies. Related to Figure 2.
1220
1221 **Supp. Table 2:** Top 100 proteins that are differentially immunoprecipitated with the HA
1222 antibody in SINV-infected vs mock-infected FHA:DICER cells. Related to Figure 2.
1223
1224 **Supp. Table 3:** Top 100 proteins that are differentially immunoprecipitated in mock-infected
1225 FHA:DICER cells by the HA and Myc (CTL) antibodies, in the SFV infection experiment.
1226 Related to Figure S2.
1227
1228 **Supp. Table 4:** Top 100 proteins that are differentially immunoprecipitated with the HA
1229 antibody in SFV-infected vs mock-infected FHA:DICER cells. Related to Figure S2.
1230
1231 **Supp. Table 5:** List of primers used in this study.

Figure 1

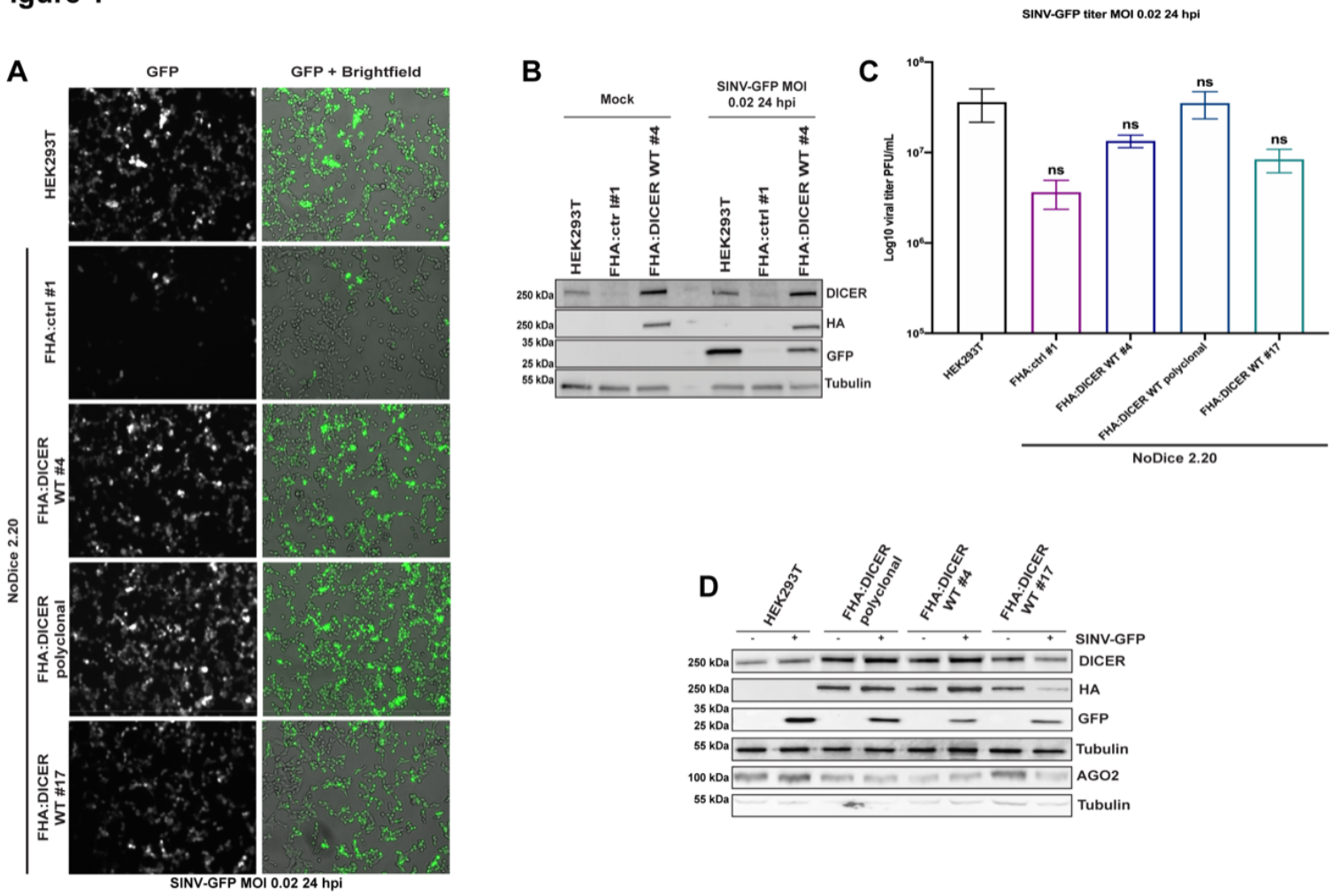
A
GFP
GFP + Brightfield
HEK293T
FHA:ctrl #1
FHA:DICER WT #4
FHA:DICER polyclonal
FHA:DICER WT #17
NoDice 2.20
SINV-GFP MOI 0.02 24 hpi
B
Mock
SINV-GFP MOI 0.02 24 hpi
HEK293T
FHA:ctr l#1
FHA:DICER WT #4
HEK293T
FHA:ctrl #1
FHA:DICER WT #4
250 kDa
250 kDa
35 kDa
25 kDa
55 kDa
DICER
HA
GFP
Tubulin
C
SINV-GFP titer MOI 0.02 24 hpi
Log10 viral titer PFU/mL
ns
HEK293T
FHA:ctrl #1
FHA:DICER WT #4
FHA:DICER WT polyclonal
FHA:DICER WT #17
NoDice 2.20
D
HEK293T
FHA:DICER polyclonal
FHA:DICER WT #4
FHA:DICER WT #17
SINV-GFP
250 kDa
250 kDa
35 kDa
25 kDa
55 kDa
100 kDa
55 kDa
DICER
HA
GFP
Tubulin
AGO2
Tubulin

Figure 2

A

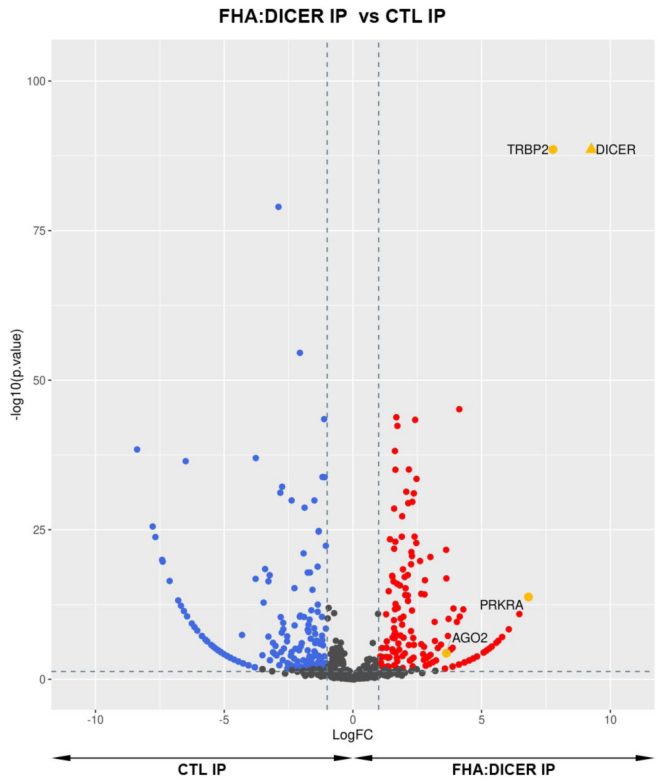

B

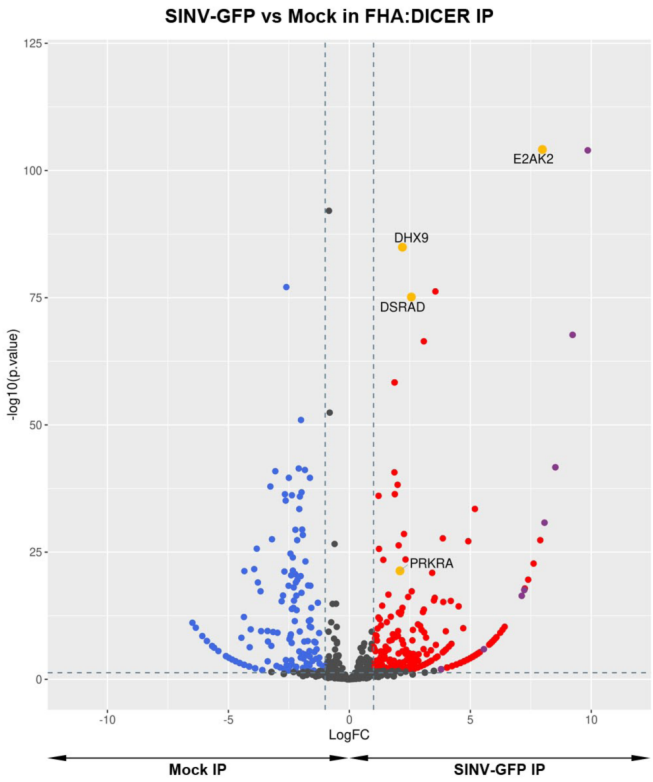

C

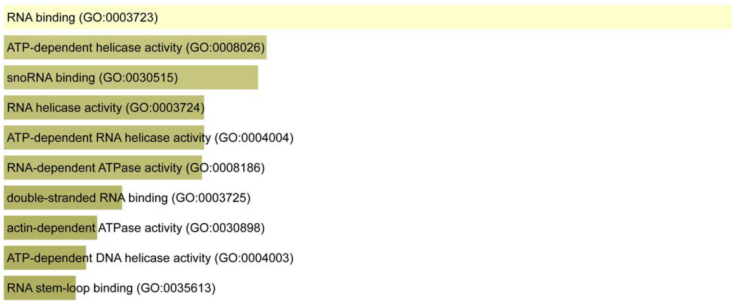

D

Gene name	Mean spectral count		LogFC	Adjusted p-value
	SINV-GFP IP	MOCK IP		
E2AK2 (PKR)	123.3	0.3	7.979	7.316e-102
DSRAD (ADAR-1)	181.3	28.3	2.563	1.421e-73
DHX9	247.3	50	2.194	4.012e-83
PRKRA (PACT)	63.3	13.7	2.093	1.158e-20

Figure 3

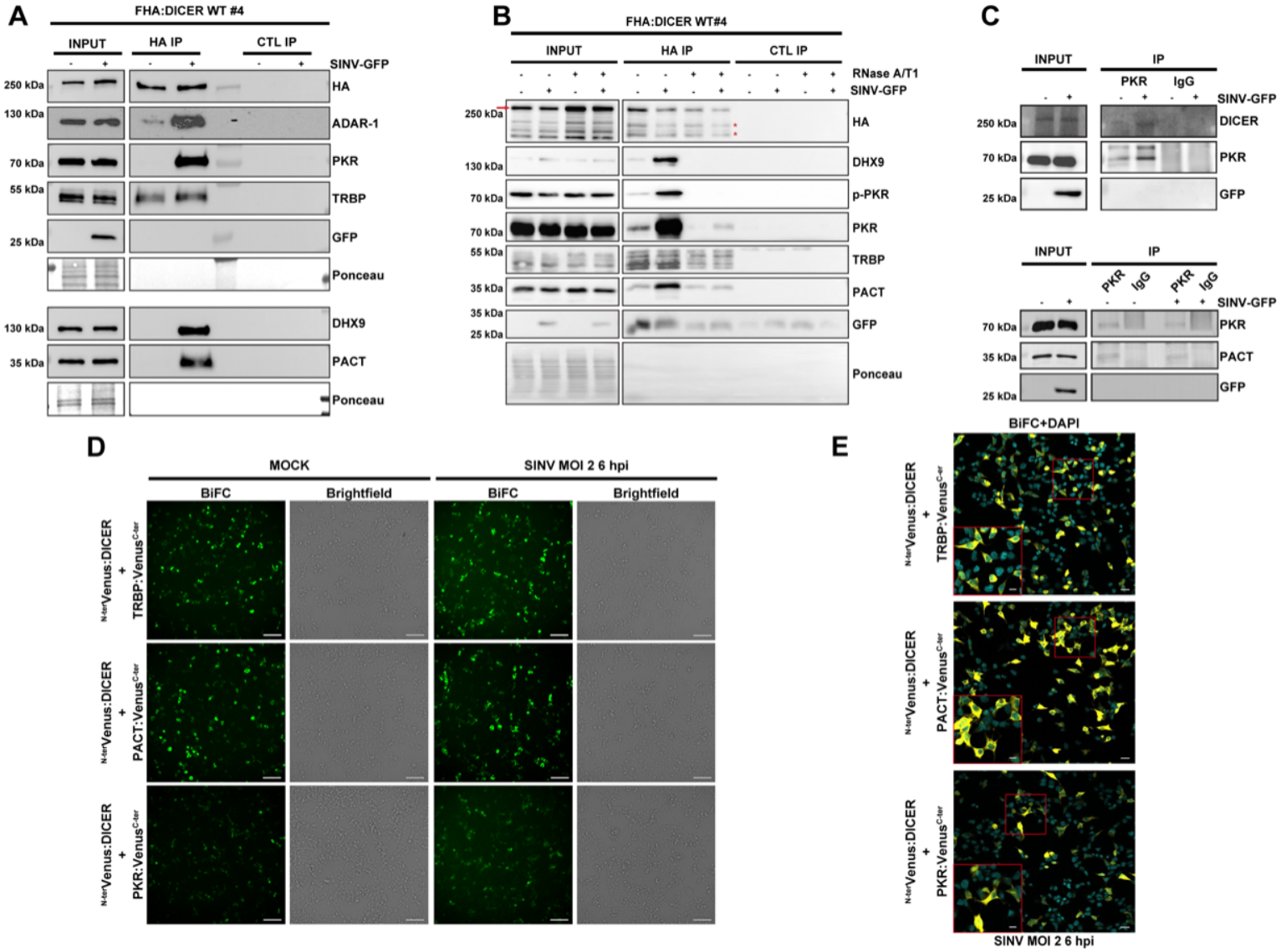
A
FHA:DICER WT #4
INPUT
HA IP
CTL IP
SINV-GFP
250 kDa
HA
130 kDa
ADAR-1
70 kDa
PKR
55 kDa
TRBP
25 kDa
GFP
Ponceau
130 kDa
DHX9
35 kDa
PACT
Ponceau
B
FHA:DICER WT#4
INPUT
HA IP
CTL IP
RNase A/T1
SINV-GFP
250 kDa
HA
130 kDa
DHX9
70 kDa
p-PKR
70 kDa
PKR
55 kDa
TRBP
35 kDa
PACT
35 kDa
25 kDa
GFP
Ponceau
C
INPUT
IP
PKR
IgG
SINV-GFP
250 kDa
DICER
70 kDa
PKR
25 kDa
GFP
INPUT
IP
PKR
IgG
PKR
IgG
SINV-GFP
70 kDa
PKR
35 kDa
PACT
25 kDa
GFP
D
MOCK
SINV MOI 2 6 hpi
BiFC
Brightfield
BiFC
Brightfield
N-terVenus:DICER + TRBP:VenusC-ter
N-terVenus:DICER + PACT:VenusC-ter
N-terVenus:DICER + PKR:VenusC-ter
E
BiFC+DAPI
N-terVenus:DICER + TRBP:VenusC-ter
N-terVenus:DICER + PACT:VenusC-ter
N-terVenus:DICER + PKR:VenusC-ter
SINV MOI 2 6 hpi

Figure 4

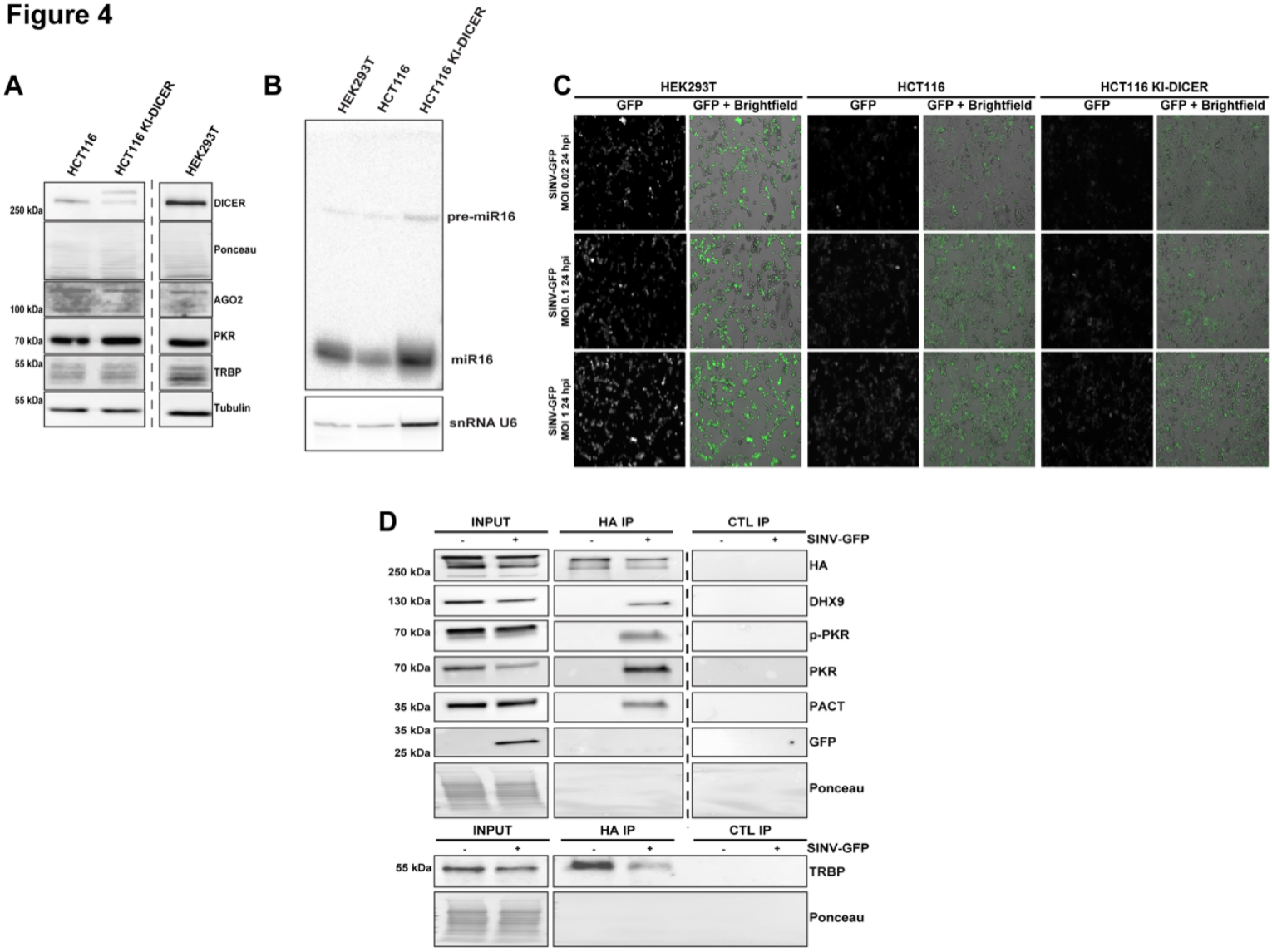
A
HCT116
HCT116 KI-DICER
HEK293T
250 kDa
DICER
Ponceau
100 kDa
AGO2
70 kDa
PKR
55 kDa
TRBP
55 kDa
Tubulin
B
HEK293T
HCT116
HCT116 KI-DICER
pre-miR16
miR16
snRNA U6
C
HEK293T
HCT116
HCT116 KI-DICER
GFP
GFP + Brightfield
SINV-GFP MOI 0.02 24 hpi
SINV-GFP MOI 0.1 24 hpi
SINV-GFP MOI 1 24 hpi
D
INPUT
HA IP
CTL IP
SINV-GFP
250 kDa
HA
130 kDa
DHX9
70 kDa
p-PKR
70 kDa
PKR
35 kDa
PACT
35 kDa
25 kDa
GFP
Ponceau
55 kDa
TRBP
Ponceau

Figure 5

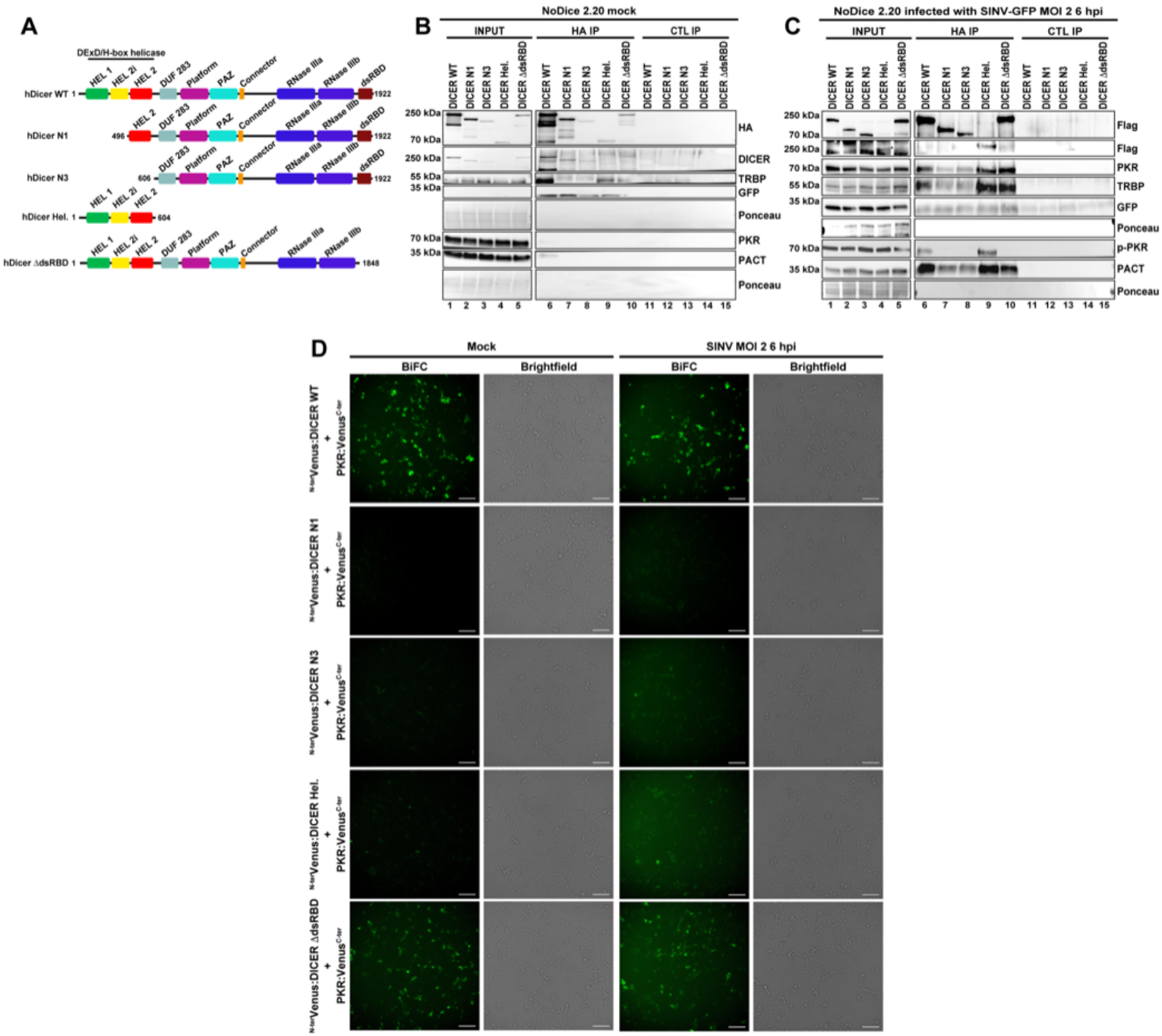
A
DExD/H-box helicase
HEL 1
HEL 2i
HEL 2
DUF 283
Platform
PAZ
Connector
RNase IIIa
RNase IIIb
dsRBD
hDicer WT 1
1922
hDicer N1
496
hDicer N3
606
hDicer Hel. 1
604
hDicer ΔdsRBD 1
1848
B
NoDice 2.20 mock
INPUT
HA IP
CTL IP
DICER WT
DICER N1
DICER N3
DICER Hel.
DICER ΔdsRBD
250 kDa
70 kDa
55 kDa
35 kDa
HA
DICER
TRBP
GFP
Ponceau
PKR
PACT
C
NoDice 2.20 infected with SINV-GFP MOI 2 6 hpi
Flag
p-PKR
D
Mock
SINV MOI 2 6 hpi
BiFC
Brightfield
N-terVenus:DICER WT
N-terVenus:DICER N1
N-terVenus:DICER N3
N-terVenus:DICER Hel.
N-terVenus:DICER ΔdsRBD
PKR:VenusC-ter

Figure 6

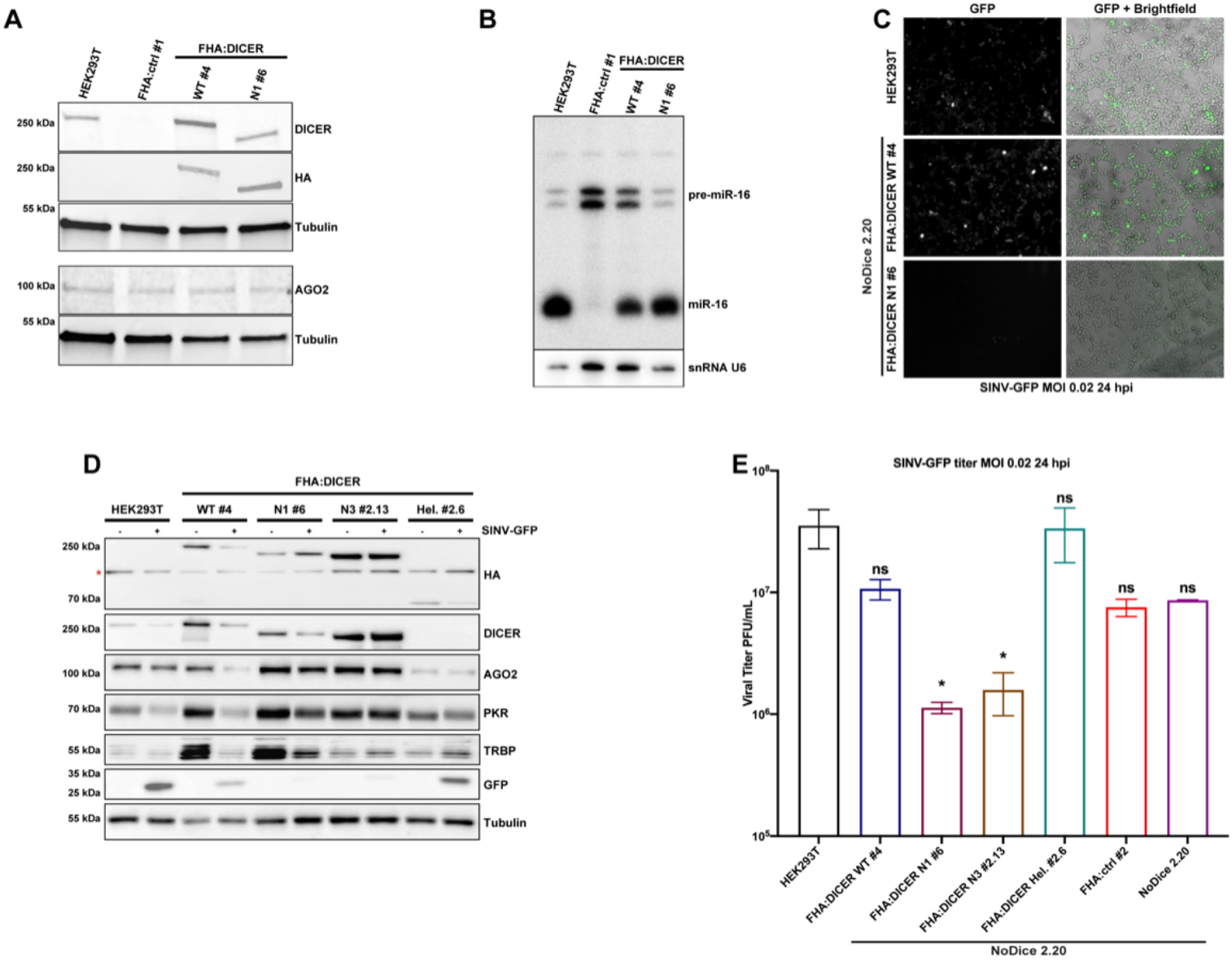
A
HEK293T
FHA:ctrl #1
FHA:DICER
WT #4
N1 #6
250 kDa
DICER
250 kDa
HA
55 kDa
Tubulin
100 kDa
AGO2
55 kDa
Tubulin
B
HEK293T
FHA:ctrl #1
FHA:DICER
WT #4
N1 #6
pre-miR-16
miR-16
snRNA U6
C
GFP
GFP + Brightfield
HEK293T
NoDice 2.20
FHA:DICER WT #4
FHA:DICER N1 #6
SINV-GFP MOI 0.02 24 hpi
D
FHA:DICER
HEK293T
WT #4
N1 #6
N3 #2.13
Hel. #2.6
SINV-GFP
250 kDa
HA
70 kDa
250 kDa
DICER
100 kDa
AGO2
70 kDa
PKR
55 kDa
TRBP
35 kDa
25 kDa
GFP
55 kDa
Tubulin
E
SINV-GFP titer MOI 0.02 24 hpi
Viral Titer PFU/mL
ns
*
HEK293T
FHA:DICER WT #4
FHA:DICER N1 #6
FHA:DICER N3 #2.13
FHA:DICER Hel. #2.6
FHA:ctrl #2
NoDice 2.20
NoDice 2.20

Figure S1

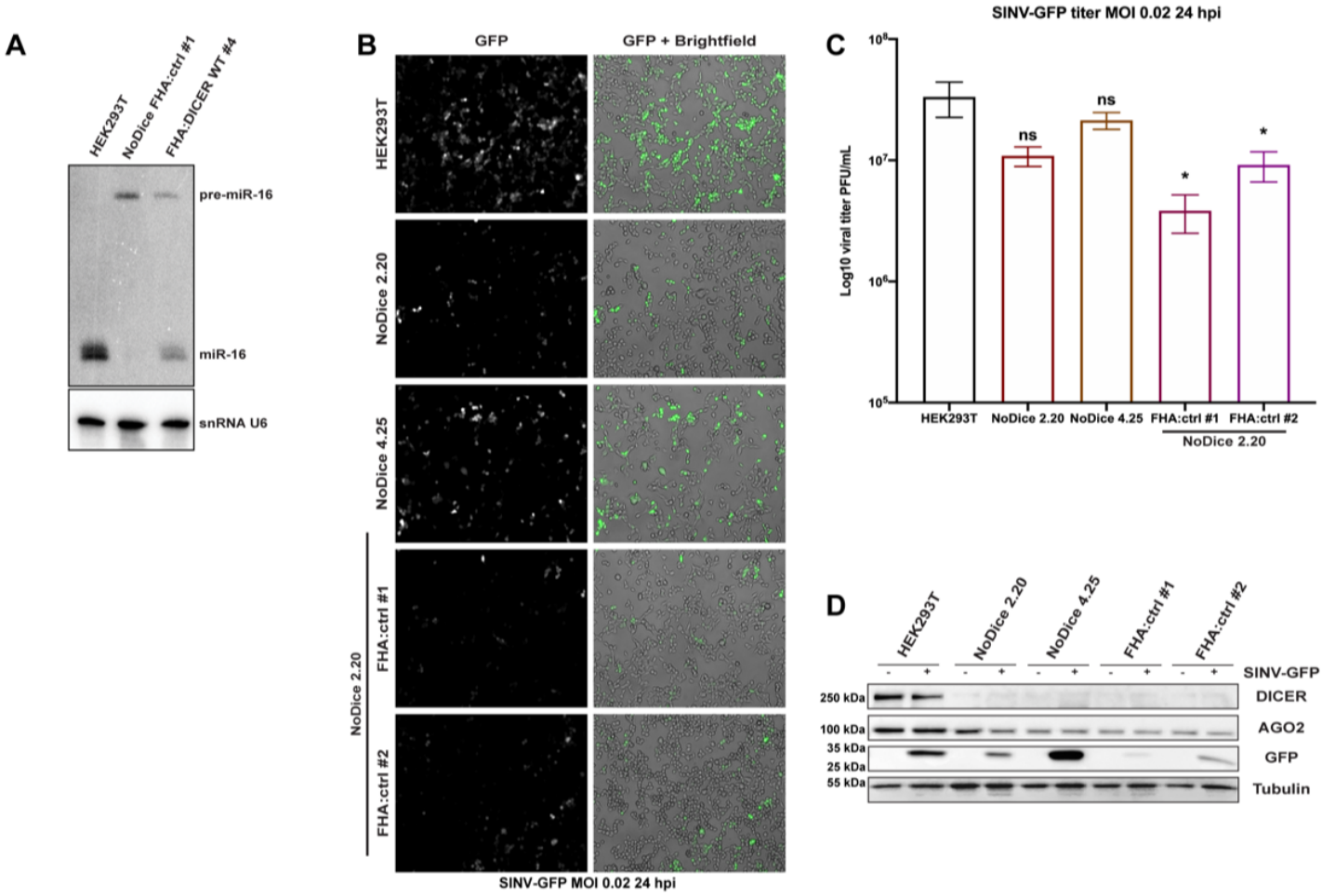
A
HEK293T
NoDice FHA:ctrl #1
FHA:DICER WT #4
pre-miR-16
miR-16
snRNA U6
B
GFP
GFP + Brightfield
HEK293T
NoDice 2.20
NoDice 4.25
NoDice 2.20
FHA:ctrl #1
FHA:ctrl #2
SINV-GFP MOI 0.02 24 hpi
C
SINV-GFP titer MOI 0.02 24 hpi
Log10 viral titer PFU/mL
ns
ns
*
*
HEK293T
NoDice 2.20
NoDice 4.25
FHA:ctrl #1
FHA:ctrl #2
NoDice 2.20
D
HEK293T
NoDice 2.20
NoDice 4.25
FHA:ctrl #1
FHA:ctrl #2
SINV-GFP
250 kDa
DICER
100 kDa
AGO2
35 kDa
25 kDa
GFP
55 kDa
Tubulin

Figure S2

A

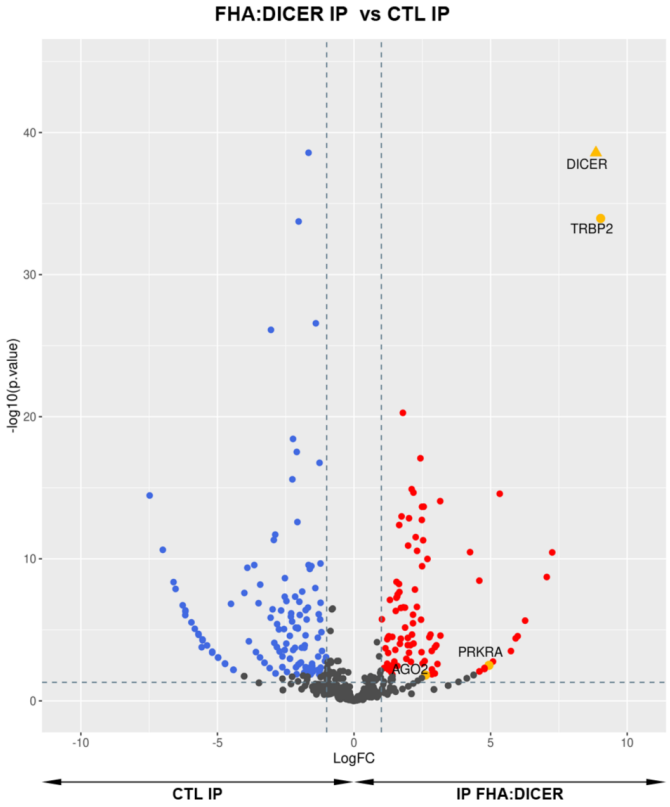

B

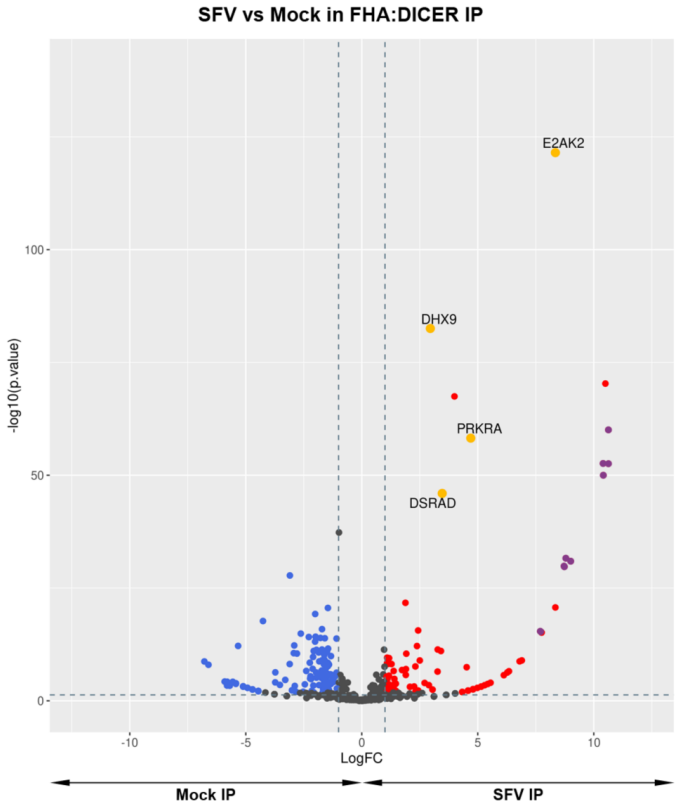

C

Gene name	Mean spectral count		LogFC	Adjusted p-value
	SFV IP	Mock IP		
E2AK2 (PKR)	221	0.5	8.344	2.611e-119
PRKRA (PACT)	131.5	4.5	4.697	8.415e-57
DSRAD (ADAR-1)	268	22	3.466	9.118e-45
DHX9	265	31	2.955	1.245e-80

Figure S3

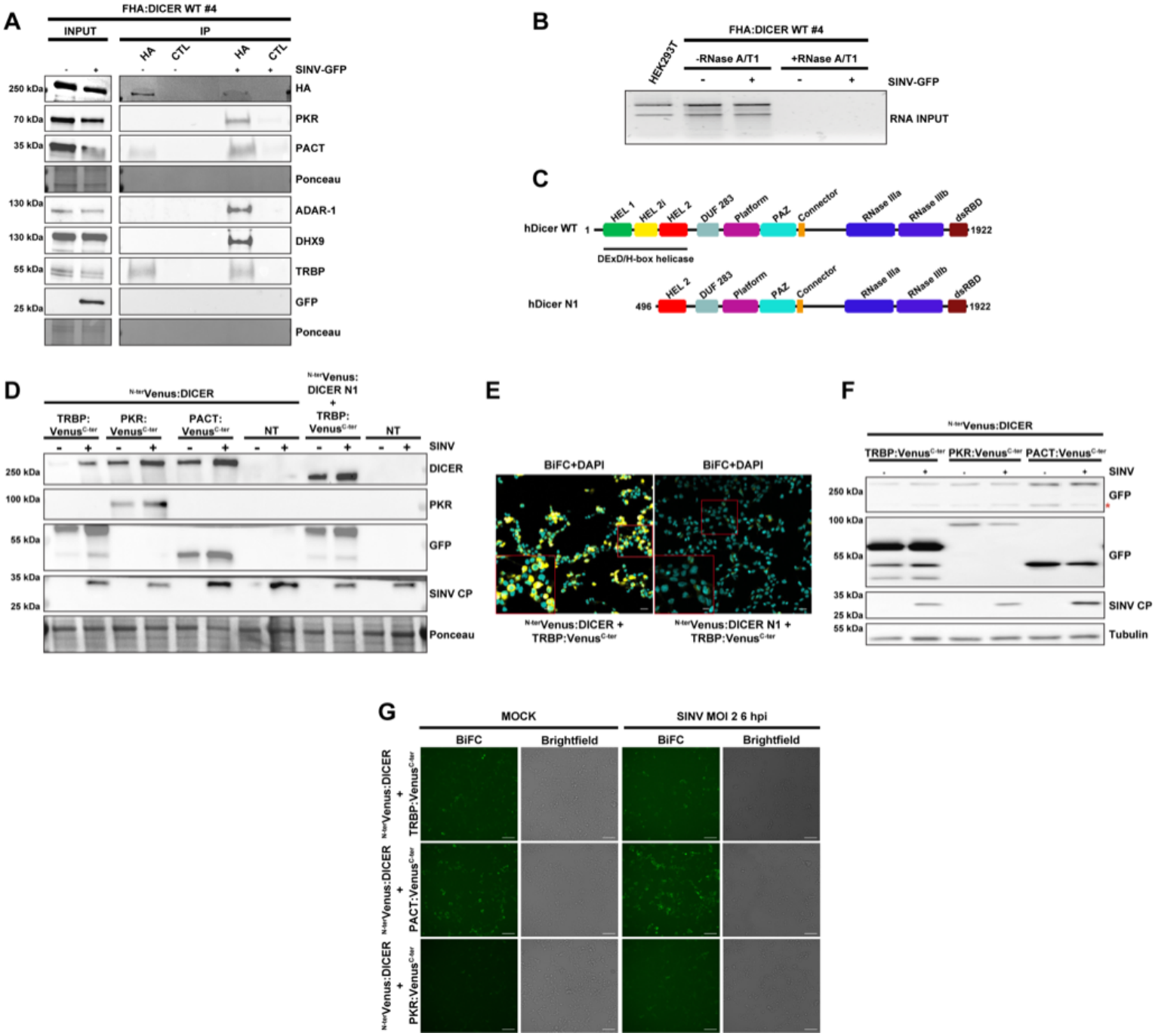
A
FHA:DICER WT #4
INPUT
IP
HA
CTL
HA
CTL
SINV-GFP
250 kDa
HA
70 kDa
PKR
35 kDa
PACT
Ponceau
130 kDa
ADAR-1
130 kDa
DHX9
55 kDa
TRBP
25 kDa
GFP
Ponceau
B
FHA:DICER WT #4
HEK293T
-RNase A/T1
+RNase A/T1
SINV-GFP
RNA INPUT
C
hDicer WT
HEL 1
HEL 2i
HEL 2
DUF 283
Platform
PAZ
Connector
RNase IIIa
RNase IIIb
dsRBD
1922
DExD/H-box helicase
hDicer N1
496
HEL 2
DUF 283
Platform
PAZ
Connector
RNase IIIa
RNase IIIb
dsRBD
1922
D
N-terVenus:DICER
N-terVenus: DICER N1 + TRBP: VenusC-ter
TRBP: VenusC-ter
PKR: VenusC-ter
PACT: VenusC-ter
NT
NT
SINV
250 kDa
DICER
100 kDa
PKR
55 kDa
GFP
35 kDa
SINV CP
25 kDa
Ponceau
E
BiFC+DAPI
BiFC+DAPI
N-terVenus:DICER + TRBP:VenusC-ter
N-terVenus:DICER N1 + TRBP:VenusC-ter
F
N-terVenus:DICER
TRBP:VenusC-ter
PKR:VenusC-ter
PACT:VenusC-ter
SINV
250 kDa
GFP
100 kDa
55 kDa
GFP
35 kDa
SINV CP
25 kDa
55 kDa
Tubulin
G
MOCK
SINV MOI 2 6 hpi
BiFC
Brightfield
BiFC
Brightfield
N-terVenus:DICER + TRBP:VenusC-ter
N-terVenus:DICER + PACT:VenusC-ter
N-terVenus:DICER + PKR:VenusC-ter

Figure S4

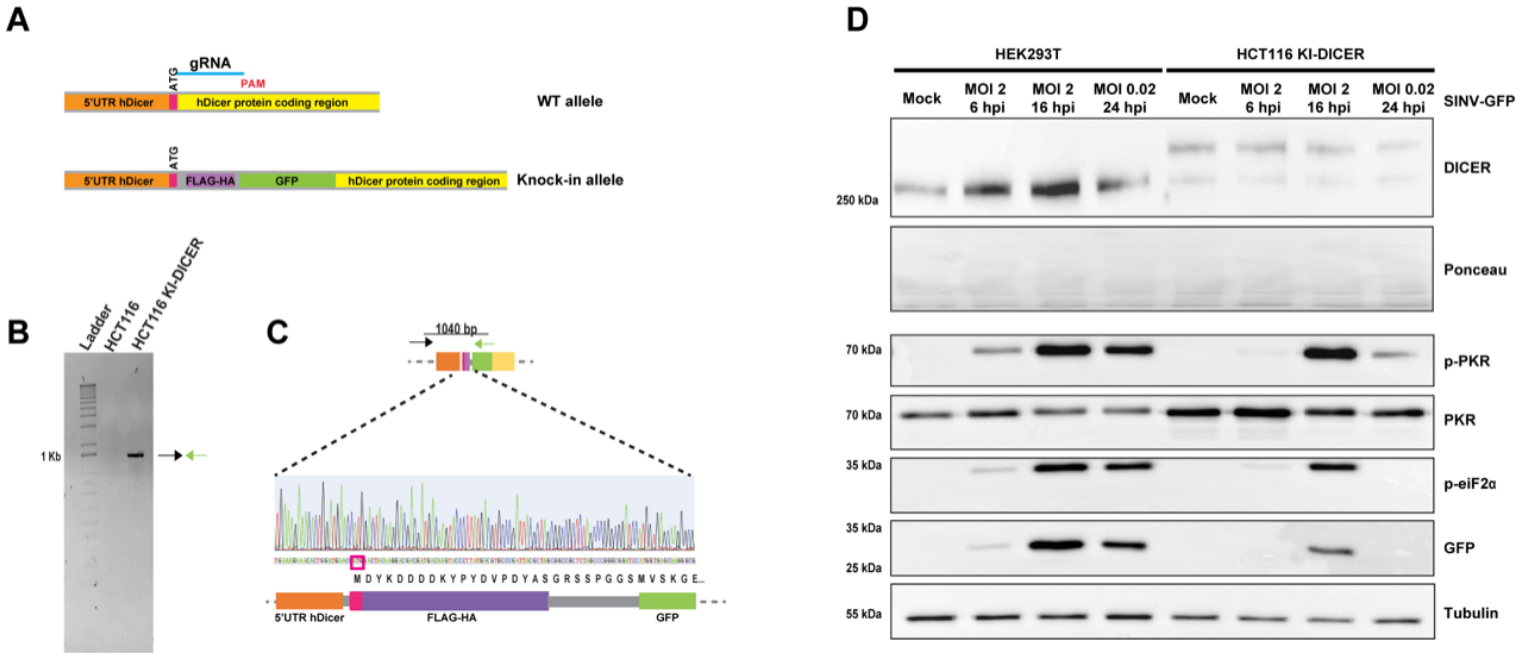
A
gRNA
ATG
PAM
5'UTR hDicer
hDicer protein coding region
WT allele
ATG
5'UTR hDicer
FLAG-HA
GFP
hDicer protein coding region
Knock-in allele
B
Ladder
HCT116
HCT116 KI-DICER
1 Kb
C
1040 bp
M D Y K D D D D K Y P Y D V P D Y A S G R S S P G G S M V S K G E...
5'UTR hDicer
FLAG-HA
GFP
D
HEK293T
HCT116 KI-DICER
Mock
MOI 2 6 hpi
MOI 2 16 hpi
MOI 0.02 24 hpi
Mock
MOI 2 6 hpi
MOI 2 16 hpi
MOI 0.02 24 hpi
SINV-GFP
250 kDa
DICER
Ponceau
70 kDa
p-PKR
70 kDa
PKR
35 kDa
p-eiF2α
35 kDa
25 kDa
GFP
55 kDa
Tubulin

Figure S5

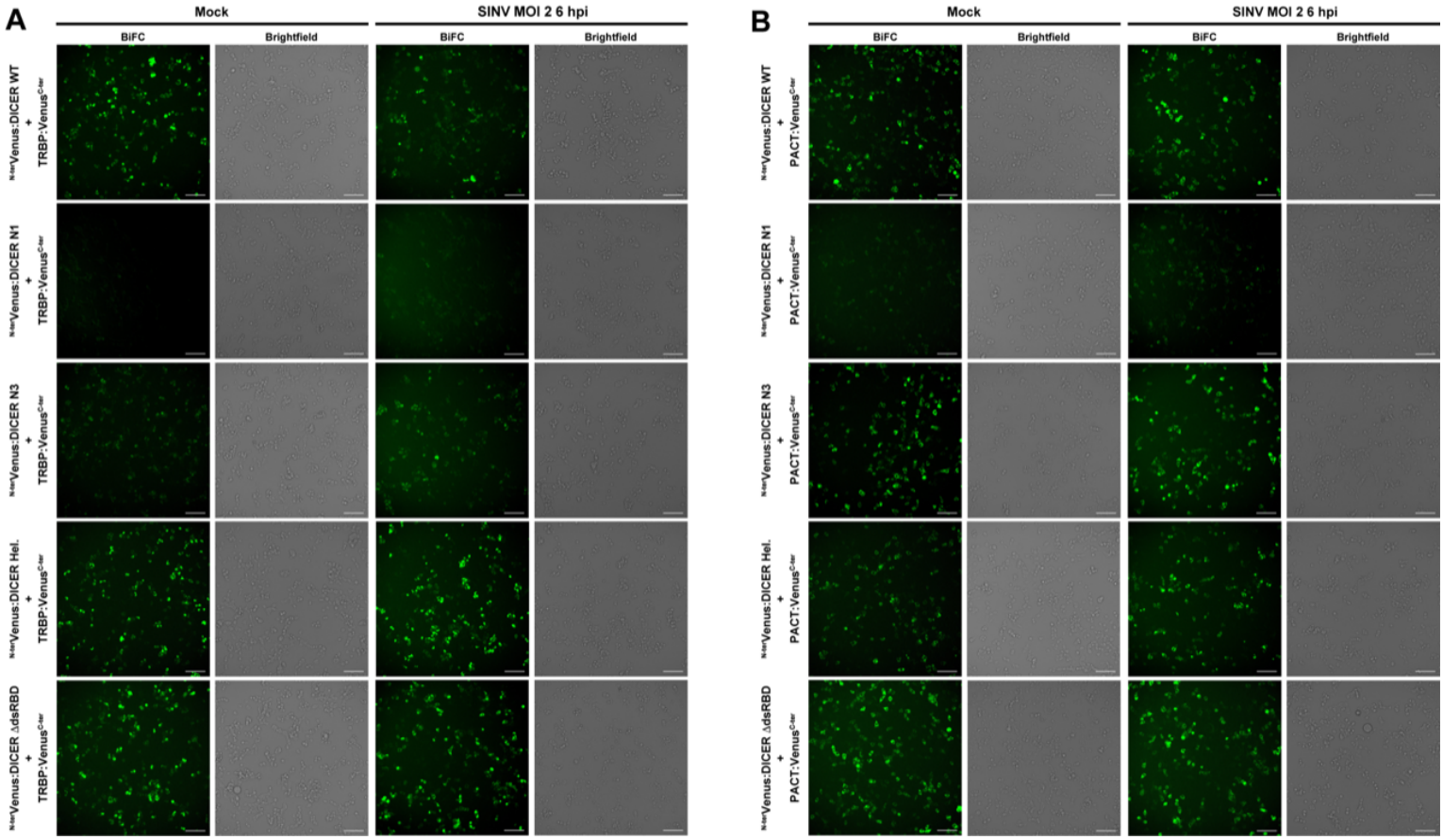
A
Mock
SINV MOI 2 6 hpi
BiFC
Brightfield
BiFC
Brightfield
N-terVenus:DICER WT + TRBP:Venus C-ter
N-terVenus:DICER N1 + TRBP:Venus C-ter
N-terVenus:DICER N3 + TRBP:Venus C-ter
N-terVenus:DICER Hel. + TRBP:Venus C-ter
N-terVenus:DICER ΔdsRBD + TRBP:Venus C-ter
B
Mock
SINV MOI 2 6 hpi
BiFC
Brightfield
BiFC
Brightfield
N-terVenus:DICER WT + PACT:Venus C-ter
N-terVenus:DICER N1 + PACT:Venus C-ter
N-terVenus:DICER N3 + PACT:Venus C-ter
N-terVenus:DICER Hel. + PACT:Venus C-ter
N-terVenus:DICER ΔdsRBD + PACT:Venus C-ter

Figure S6

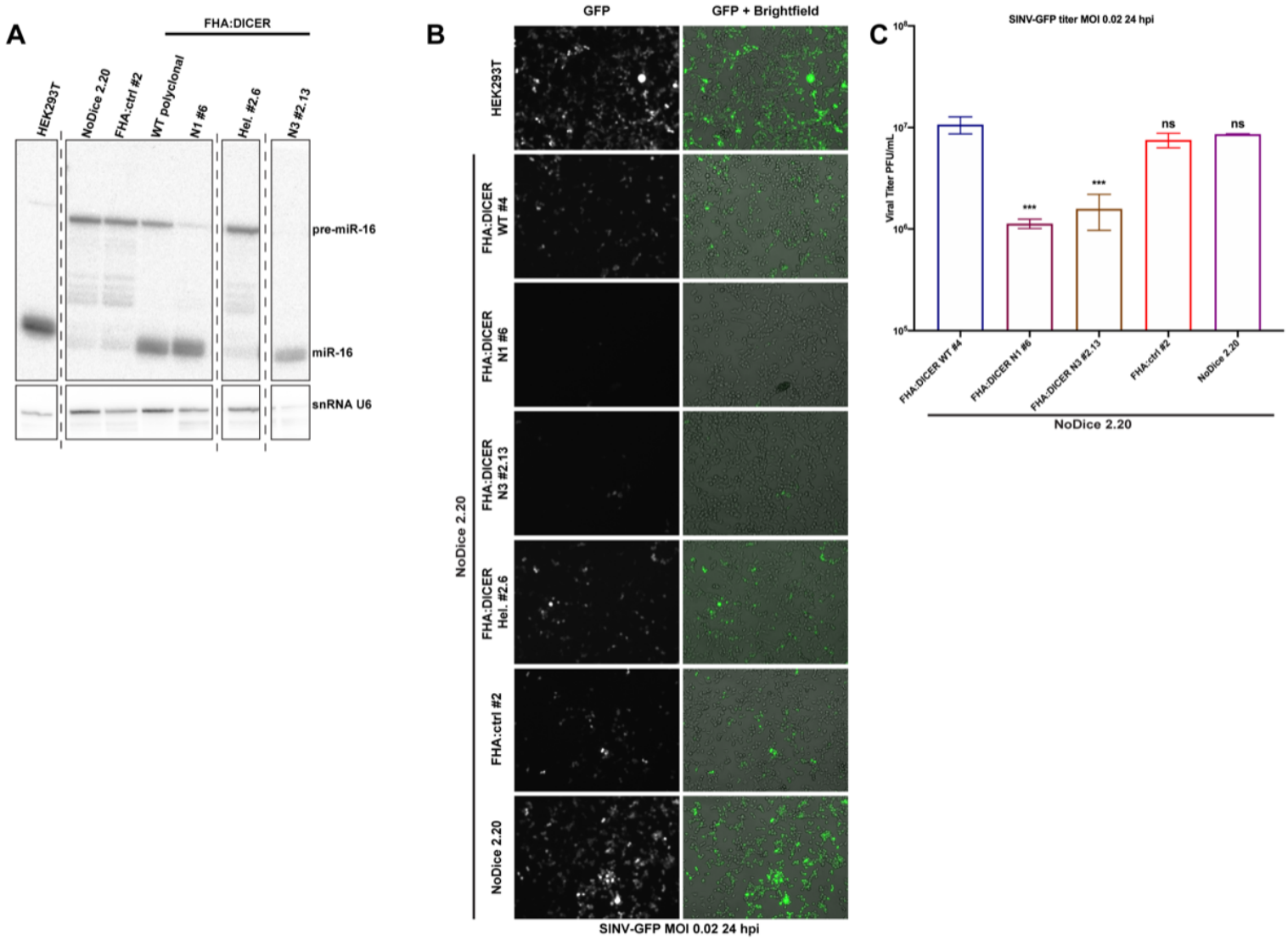
A
FHA:DICER
HEK293T
NoDice 2.20
FHA:ctrl #2
WT polyclonal
N1 #6
Hel. #2.6
N3 #2.13
pre-miR-16
miR-16
snRNA U6
B
GFP
GFP + Brightfield
HEK293T
FHA:DICER WT #4
FHA:DICER N1 #6
FHA:DICER N3 #2.13
FHA:DICER Hel. #2.6
FHA:ctrl #2
NoDice 2.20
NoDice 2.20
SINV-GFP MOI 0.02 24 hpi
C
SINV-GFP titer MOI 0.02 24 hpi
Viral Titer PFU/mL
10^8
10^7
10^6
10^5
***
***
ns
ns
FHA:DICER WT #4
FHA:DICER N1 #6
FHA:DICER N3 #2.13
FHA:ctrl #2
NoDice 2.20
NoDice 2.20